Seabed Scour and Buried-Pipeline Deformation Due to Ice Ridges: Pipeline Stress and Deformation

Quarterly Progress Report I

by

Hossein Fadaifard

Ph.D. Candidate

The University of Texas at Austin

Supervised

by

John L. Tassoulas

Sponsored

by

DOI/BOEMRE

Order: M11PX00128

COR: Zachary Scott

CA: Rebecca L. Kruse

December 7, 2011

Preface

This report summarizes our progress to date (first quarter) in the Project entitled “Seabed Scour and Buried-Pipeline Deformation Due to Ice Ridges: Pipeline Stress and Deformation”. The work has proceeded as planned. We have developed and implemented a computational procedure based on the finite element method suitable for the analysis of fluid-structure interaction problems. Furthermore, we have verified the validity of the implementation by comparison with available documented solutions to test problems. We have dealt with several computational challenges successfully and expect to resolve the remaining issues during the second quarter of the Project.

1 Introduction

In this report, we aim to summarize a unified approach for solving fluid-structure interaction (FSI) problems using finite element methods (FEM).

An Eulerian framework is commonly used for describing fluid flow, while for the structures (solids), a Lagrangian description is seems natural. The inherent problem of coupled fluid-structure interaction problems lies in the inconsistent frameworks used to describe the two media.

A common approach in dealing with these two media has been the so-called Arbitrary Lagrangian-Eulerian (ALE) method. Within the ALE framework the governing equations of the solid are left in their natural Lagrangian setting while an arbitrary frame of is taken for describing the fluid such that contact between the fluid and the structure is maintained throughout the course of the analysis.

Consider the problem of an elastic beam attached to a rigid cylinder as shown in Figure 1.0.1a. Initially, the fluid (empty grids) and the structure have meshes conforming at the nodal points on the boundary of the solid. Suppose the structure moves to its new equilibrium position shown in Figure 1.0.1b. After deforming, the contact between the fluid nodes and the solid nodes is lost.

In ALE formulations, the fluid nodal points at the interface are moved such that contact between the solid and the fluid is maintained at the interface. The remainder of the fluid nodal points "arbitrary" (but purposeful) manner (Figure 1.0.1c). Although arbitrary, the mesh movement has to satisfy the following criteria:

1. "Good" elements must be produced after movement of the fluid mesh. Good elements are those that have "nice" aspect ratios.

2. No folding over of elements occurs at any point in the mesh.

Depending on the formulation taken, the movement of the mesh may be further restricted due to the so-called geometric conservation law [9] (GCL) which requires the solution of a constant field to be preserved exactly in moving domains.

Here, we group procedures between the fluid and the solid can be grouped as either *partitioned* or a *monolithic*, the description of which follows:

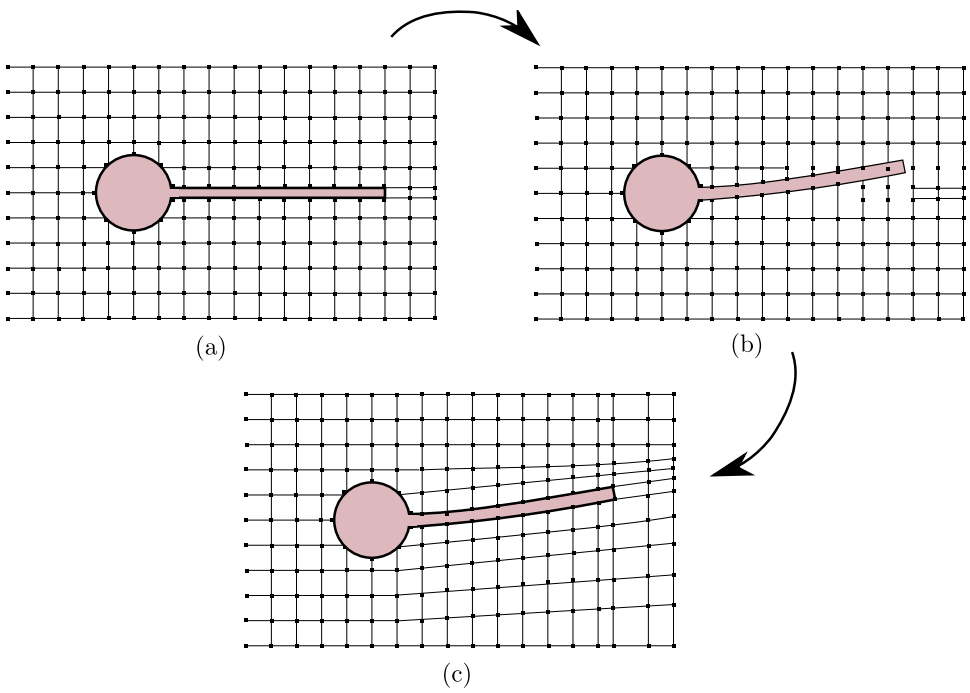

Figure 1.0.1: ALE procedure

1. **Monolithic**: The full system of equations are solved simultaneously. In the case of 2D problems, this involves solving 6 equations simultaneously: 4 momentum equations (2 for fluid, and 2 for solid), 1 continuity equation for fluid, and 1 mesh updating equation.

2. **Partitioned**:

   (i) **Loosely coupled**: For a given time-step, the fluid equations are solved assuming the displacements of the solid are known. The forces on the structure are then transferred to a solid solver and the displacements of the structure are solved for. Fluid mesh is updated based on the displacements of the structure, and a new time-step is started.

   (ii) **Strongly coupled**: This is exactly the same as the loosely coupled algorithm with the exception that iterations are carried out between the solution of the fluid and the solid until convergence of the equilibrium forces at the final configurations are satisfied [7]. See Figure 1.0.2.

Partitioned schemes suffer from poor convergence rates, and even failure to converge to a solution. These approaches are further susceptible to the so-called instabilities due to "added mass effect" (See for instance [4]).

The downsides of the monolithic algorithms are the associated huge computational costs. Making such algorithms parallel is far from straight forward due to the inherently ill-conditioned final systems of equations.

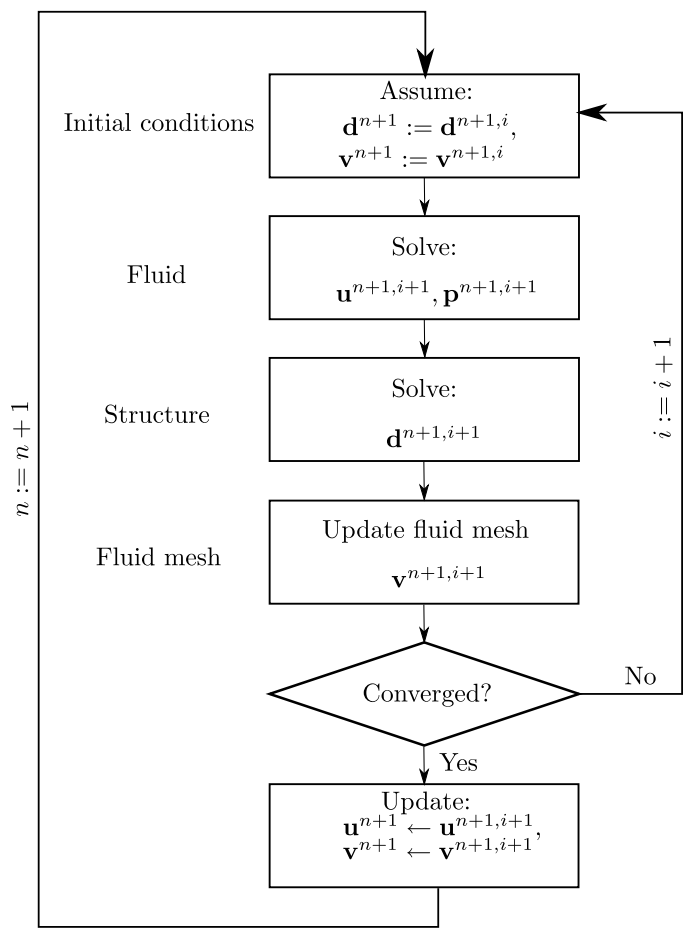

Figure 1.0.2: Strongly coupled FSI algorithm. Superscript n denotes time-step count, and i denotes iteration number. $\mathbf{d}$ denotes structural displacements, $\mathbf{u}$ denotes fluid velocities, and $\mathbf{v}$ denotes mesh velocity.

2 A Model Problem

Consider the scalar advection-diffusion problem presented as a segue to the discussion of the incompressible Navier-Stokes equations on moving domains. The initial boundary-value problem (IBVP) on a non-moving domain is stated as follows: find $\phi(\mathbf{x}, t)$ such that

$$\phi_t + \mathbf{u}(\mathbf{x}, t) \cdot \nabla_{\mathbf{x}} \phi - \mu(\mathbf{x}) \Delta_{\mathbf{x}} \phi = f(\mathbf{x}, t), \quad \text{in} \quad \Omega(t) \times]0, T[, \tag{2.1}$$

$$\phi(\mathbf{x}, 0) = \phi^o \quad \text{in} \quad \Omega(0) \times 0, \tag{2.2}$$

$$\phi(\mathbf{x}, t) = g(\mathbf{x}, t) \quad \text{in} \quad \partial\Omega(t) \times]0, T[, \tag{2.3}$$

where $\mathbf{u}$ and μ are smooth solenoidal vector-valued and scalar-valued point functions, respectively, and $\Delta_{\mathbf{x}}$ denotes the Laplacian taken with respect to $\mathbf{x}$.

Consider a fixed configuration $\mathcal{R}_{\boldsymbol{\chi}}$ hereon termed as the reference configuration. Denote by $\boldsymbol{\chi} \in \mathcal{R}_{\boldsymbol{\chi}}$ the coordinates of this configuration, and let Ψ be the one-to-one mapping from the referential frame to the spacial one (Figure 2.0.3). This mapping is described as

$$\Psi = \begin{cases} R_{\boldsymbol{\chi}} \times [0, T] & \longrightarrow R_{\mathbf{x}} \times [0, T] \\ (\boldsymbol{\chi}, t) & \longrightarrow (\mathbf{x}, t). \end{cases} \tag{2.4}$$

Noting that $\phi(\mathbf{x}, t) = \phi \circ \Psi$, we have

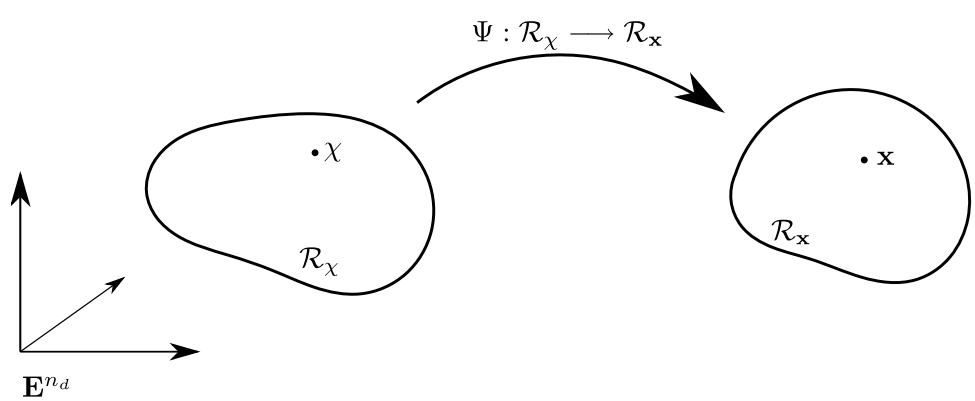

Figure 2.0.3: Mapping between referential and spatial configurations

$$\frac{\partial \phi}{\partial t}\Big|_{\boldsymbol{\chi}} = \frac{\partial \phi}{\partial t}\Big|_{\mathbf{x}} + \frac{\partial \phi}{\partial \Psi(\boldsymbol{\chi}, t)} \frac{\partial \mathbf{x}}{\partial t}\Big|_{\boldsymbol{\chi}}, \tag{2.5}$$

or

$$\frac{\partial \phi}{\partial t}\Big|_{\mathbf{x}} = \frac{\partial \phi}{\partial t}\Big|_{\boldsymbol{\chi}} - \mathbf{v} \cdot \nabla_{\mathbf{x}} \phi, \tag{2.6}$$

where we have denoted $\mathbf{v} := \frac{\partial \mathbf{x}}{\partial t}\Big|_{\boldsymbol{\chi}}$ as the velocity of the referential configuration.

Substituting the obtained expression into the strong form of the differential equation given in the previous section, we arrive at an equivalent form of the IBVP, but now written with respect to a referential configuration: find $\phi(\mathbf{x}, t)$ such that

$$\frac{\partial \phi}{\partial t}\Big|_{\boldsymbol{\chi}} + \mathbf{c}(\mathbf{x}, t) \cdot \nabla_{\mathbf{x}} \phi - \mu(\mathbf{x}) \Delta_{\mathbf{x}} \phi = f(\mathbf{x}, t), \quad \text{in} \quad \Omega \times]0, T[, \tag{2.7}$$

$$\phi(\mathbf{x}, 0) = \phi^o \quad \text{in} \quad \Omega \times 0, \tag{2.8}$$

$$\phi(\mathbf{x}, t) = g(\mathbf{x}, t) \quad \text{in} \quad \partial\Omega \times]0, T[, \tag{2.9}$$

where, $\mathbf{c} := \mathbf{u} - \mathbf{v}$. Above IBVP is identical to the original advection-diffusion equation, but now written with respect to an arbitrary frame of reference. Indeed, the original equation is recovered by choosing $\Psi = id_{\mathbf{x}}$.

In the next section, we present at two different variational forms of the IBVP.

2.1 Variational Formulation and Geometric Conservation Law

Let $\mathcal{V} := \{w | w \in H_0^1(\Omega)\}$, and $\mathcal{S} := \{\phi(\cdot, t) | \phi \in H^1(\Omega), \phi(\mathbf{x}, 0) = \phi^o, \phi(\mathbf{x}, t)_{\mathbf{x} \in \partial\Omega} = g(\mathbf{x}, t)\}$ $\forall t \in]0, T[$ denote weight function and trial solution spaces, respectively. Then the first variational form is stated as follows:

Non-conservative form: Find $\phi(\mathbf{x}, t) \in \mathcal{S}$ such that

$$\left(w, \frac{\partial \phi}{\partial t}\Big|_{\boldsymbol{\chi}}\right) + \left(w, \mathbf{c} \cdot \nabla_{\mathbf{x}} \phi\right) + \left(\nabla_{\mathbf{x}} w, \mu \nabla_{\mathbf{x}} \phi\right) + \left(w, \nabla_{\mathbf{x}} \mu \cdot \nabla_{\mathbf{x}} \phi\right) = \left(w, f\right) \quad \forall w \in \mathcal{V}. \tag{2.10}$$

Alternatively, the conservative form of the above variational form can be created as follows. Recall the Reynolds transport theorem for a function $f(\mathbf{x}, t)$

$$\frac{d}{dt}\int_{\Omega(t)} f(\mathbf{x}, t)\, d\mathbf{x} = \int_{\Omega(t)} \left(\frac{\partial f}{\partial t}\Big|_{\mathbf{x}} + \nabla_{\mathbf{x}} \cdot (f\mathbf{v}) \right) d\mathbf{x} \tag{2.11}$$

$$= \int_{\Omega(t)} \left(\frac{\partial f}{\partial t}\Big|_{\boldsymbol{\chi}} + f\nabla_{\mathbf{x}} \cdot \mathbf{v} \right) d\mathbf{x}. \tag{2.12}$$

Using these results and noting that the weight functions are time-independent, a slightly different form of the variational form follows:

Conservative form: Find $\phi(\mathbf{x}, t) \in \mathcal{S}$ such that

$$\frac{d}{dt}\Big(w, \phi_t\Big) - \Big(w, \phi\nabla_{\mathbf{x}} \cdot \mathbf{v}\Big) + \Big(w,\, \mathbf{c} \cdot \nabla_{\mathbf{x}}\phi\Big) + \Big(\nabla_{\mathbf{x}} w, \mu\nabla_{\mathbf{x}}\phi\Big) + \Big(w, \nabla_{\mathbf{x}}\mu \cdot \nabla_{\mathbf{x}}\phi\Big) = \Big(w, f\Big) \quad \forall w \in \mathcal{V}. \tag{2.13}$$

Remarks:

1. Variational formulations of the Navier-Stokes equations based on both the conservative and the non-conservative methods can be found. If finite-volume methods (FVM) are to be used for solving the governing equations, the conservative form must be used.

2. A formulation which is able to exactly reproduce a constant solution on a moving domain is said to satisfy the Geometric Conservation Law (GCL). If $\phi(\mathbf{x}, t)$ is constant in space and time, then the first variational formulation given in Eq. (2.10) recovers the exact solution.

3. For a constant ϕ, the second variational formulation given in Eq. (2.13) reduces to

$$\frac{d}{dt}\Big(w, \phi_t\Big) = \Big(w, \phi\nabla_{\mathbf{x}} \cdot \mathbf{v}\Big). \tag{2.14}$$

Thus, under the conservative formulation, a constraint on the divergence of the referential velocity exists if the formulation is to satisfy GCL. Therefore, when written in conservative form, care must be exercised when constructing the velocity field $\mathbf{v}$ (See, for instance, [2] and [3]).

2.2 Discretization and solution strategy

The non-conservative form of the variational formulation is used as a starting point for discretization. Let $\mathcal{V}^h := \{w^h | w^h \in H_0^1(\Omega)\}$, and $\mathcal{S}^h := \{\phi(\cdot, t)^h | \phi^h \in H^1(\Omega), \phi^h(\mathbf{x}, 0) = \phi^o, \phi^h(\mathbf{x}, t) = g(\mathbf{x}, t) \forall \mathbf{x} \in \partial\Omega\} \ \forall t \in]0, T[$ denote the finite-dimensional weight function and trial solution spaces, respectively. Then the formulation based on the Galerkin Finite Element Method (GFEM) reads: Find $\phi^h(\mathbf{x}, t) \in \mathcal{S}^h$ such that

$$\left(w^h, \frac{\partial \phi}{\partial t}\Big|_{\boldsymbol{\chi}}\right) + \left(w^h, \mathbf{c} \cdot \nabla_{\mathbf{x}} \phi^h\right) + \left(\nabla_{\mathbf{x}} w^h, \mu \nabla_{\mathbf{x}} \phi^h\right) + \left(w^h, \nabla_{\mathbf{x}} \mu \cdot \nabla_{\mathbf{x}} \phi^h\right) = \left(w^h, f\right) \quad \forall w^h \in \mathcal{V}. \tag{2.15}$$

Next, discretize the weighting functions as $w^h(x) = \mathbf{N}^T(\mathbf{x})\mathbf{w}^e$ where $\mathbf{N}$ denotes an array containing piecewise continuous finite element shape functions, and $\mathbf{w}^e$ denotes the nodal values of w^h for a given element. Similarly, let $\phi(\mathbf{x}, t) = \mathbf{N}(x)^T \boldsymbol{\phi}^e(t)$ where $\phi^e(t)$ is time-dependent. FEM discretization of the GFEM formulation leads to the following systems of equations:

$$\mathbf{M}\dot{\boldsymbol{\phi}} + \mathbf{K}\boldsymbol{\phi} = \mathbf{F}, \tag{2.16}$$

where,

$$\mathbf{M} := \int_\Omega \mathbf{N}\mathbf{N}^T \, d\mathbf{x} \tag{2.17}$$

$$\mathbf{K} := \int_\Omega (\mathbf{N} c_1 \mathbf{N}_{x_1}^T + \mathbf{N} c_2 \mathbf{N}_{x_2}^T) \, d\mathbf{x} + \int_\Omega \mu (\mathbf{N}_{x_1} \mathbf{N}_{x_1}^T + \mathbf{N}_{x_2} \mathbf{N}_{x_2}^T) \, d\mathbf{x} + \int_\Omega \left(\frac{\partial \mu}{\partial x_1} \mathbf{N}\mathbf{N}_{x_1}^T + \frac{\partial \mu}{\partial x_2} \mathbf{N}\mathbf{N}_{x_2}^T \right) d\mathbf{x} \tag{2.18}$$

$$\mathbf{F} := \int_\Omega \mathbf{N} f(\mathbf{x}, t) \, d\mathbf{x} \tag{2.19}$$

Finally, for time integration, employing a one-step θ-scheme gives

$$\frac{\phi^{n+1} - \phi^n}{\Delta t} = \phi^{n+\theta} := \theta \dot{\phi}^{n+1} + (1-\theta)\dot{\phi}^n, \tag{2.20}$$

and above matrix equation can be discretized in time and written as

$$(\mathbf{M} + \theta \Delta t \mathbf{K})\, \boldsymbol{\phi}^{n+1} = \theta \Delta t \mathbf{F}^{n+1} + \mathbf{M}\left[\boldsymbol{\phi}^n + \Delta t \dot{\boldsymbol{\phi}}^n\right], \tag{2.21}$$

where $\theta \in [0, 1]$ controls the accuracy and stability of the scheme.

Remarks:

1. Choice of $\theta = 0$ and $\theta = 1$ results in the first-order explicit- and implicit-Euler schemes, respectively, whereas the choice of $\theta = 1/2$ results in the second-order accurate Crank-Nicolson scheme.

2. The order of accuracy of the overall time-integration depends on how accurately the mesh velocity $\mathbf{v}$ is evaluated. Here, we propose to use the same time-integration scheme on $\mathbf{v}$ as that used on $\dot{\boldsymbol{\phi}}$. By definition $v := \left.\frac{\partial \mathbf{x}}{\partial t}\right|_{\boldsymbol{\chi}}$. Therefore, given two successive coordinates $\mathbf{x}^n$ and $\mathbf{x}^{n+1}$, the referential configuration velocity can be approximated using the relation

$$\mathbf{v}^{n+1} = \frac{\mathbf{x}^{n+1} - \mathbf{x}^n}{\theta \Delta t} + \frac{\theta - 1}{\theta}\mathbf{v}^n, \tag{2.22}$$

   where $\theta \in (0, 1]$.

3. In regions where the solution is "advection-dominated", the GFEM solution to this equation will exhibit an oscillatory behavior about the true solution. This issue can be dealt with by mesh refinement, or via introducing stabilization terms into the differential equations.

We now proceed to generalize the procedure to describe a continua in terms of a referential configuration.

3 Basics from Continuum Mechanics

3.1 Configurations and motion

We begin our discussion of continua by introducing an abstract notion of a body $\mathcal{B}$ – an open set whose elements, $p \in \mathcal{B}$, are referred to as material particles. In order to access this abstract body, we define the bijective mapping κ between the material particles and points in space defined as

$$\kappa : \mathcal{B} \longrightarrow \mathcal{R} := \kappa(\mathcal{B}) \subset \mathbb{R}^{n_d}. \tag{3.1}$$

where n_d is the number of dimensions. Let us denote by $t \in]0, T[\subset \mathbb{R}^+$ the time interval within which we are studying the motion of the body $\mathcal{B}$. From this interval, we single out the two consecutive times $t_n, t_{n+1} \in t$, within which the body assumes configurations $\kappa_n(B) := \mathcal{R}_{\mathbf{X}}$ and $\kappa_{n+1}(B) := \mathcal{R}_{\mathbf{x}}$, referred to as the material and spatial configurations, respectively. See Figure 3.1.1.

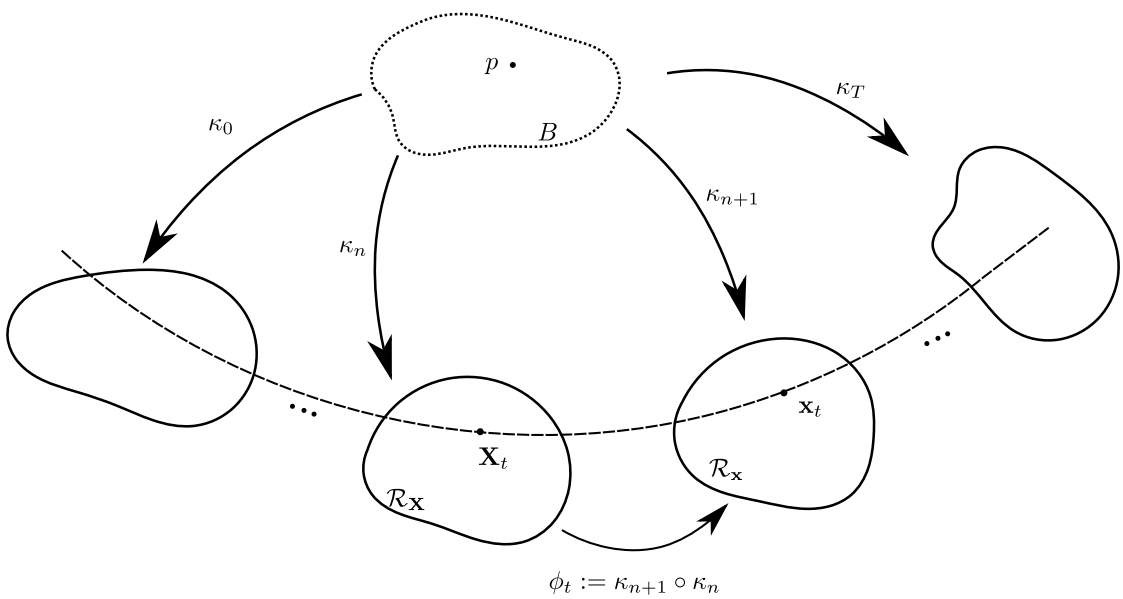

Figure 3.1.1: Motion of a material particle

We define the motion experienced by the body within the time interval $[t_n, t_{n+1}]$ as

$$\begin{aligned} \mathbf{x} &= \kappa_{n+1}(p) && (3.2)\\ &= \kappa_{n+1} \circ \kappa_n && (3.3)\\ &=: \phi_t(\mathbf{X}, t), && (3.4) \end{aligned}$$

where we've used the fact that κ is bijective. We write

$$\phi : \begin{cases} R_{\mathbf{X}} \times]0, T[& \longrightarrow R_{\mathbf{x}} \times]0, T[\ , \\ (\mathbf{X}, t) & \longrightarrow (\mathbf{x}, t), \end{cases} \tag{3.5}$$

to describe the motion experienced by the body during a time interval of interest. That is to say ϕ maps material point $\mathbf{X} = \kappa_n(p)$ to the spatial point $\mathbf{x} = \kappa_{n+1}(p)$, for the same t and interpret ϕ as describing the deformation experienced by the body during $]0, T[$. The goal of the material point is to "tag" a particular material particle, where as the spatial points give the location of the particle in the current configuration.

Consider a third configuration $\mathcal{R}_\chi$, called the referential configuration. We emphasis that the referential configuration is just that, a possibly fictitious configuration which the body may never assume, but may be convenient to choose. The mapping from $\mathcal{R}_\chi$ to $\mathcal{R}_X$ and $\mathcal{R}_x$ are denoted by Ψ, and Φ, respectively. We have

$$\Psi : \begin{cases} R_{\boldsymbol{\chi}} \times [0, T] & \longrightarrow R_X \times [0, T], \\ (\boldsymbol{\chi}, t) & \longrightarrow (\mathbf{X}, t). \end{cases} \tag{3.6}$$

and

$$\Phi : \begin{cases} R_{\boldsymbol{\chi}} \times [0, T] & \longrightarrow R_x \times [0, T], \\ (\boldsymbol{\chi}, t) & \longrightarrow (\mathbf{x}, t). \end{cases} \tag{3.7}$$

3.2 Displacement, velocity, and acceleration fields

Resorting to the referential configuration, we define the physical quantities in terms of the referential configuration. We describe the physical displacement through the referential configuration as

$$\mathbf{u}(\boldsymbol{\chi}, t) := \Phi(\boldsymbol{\chi}, t) - \Psi(\boldsymbol{\chi}, t). \tag{3.8}$$

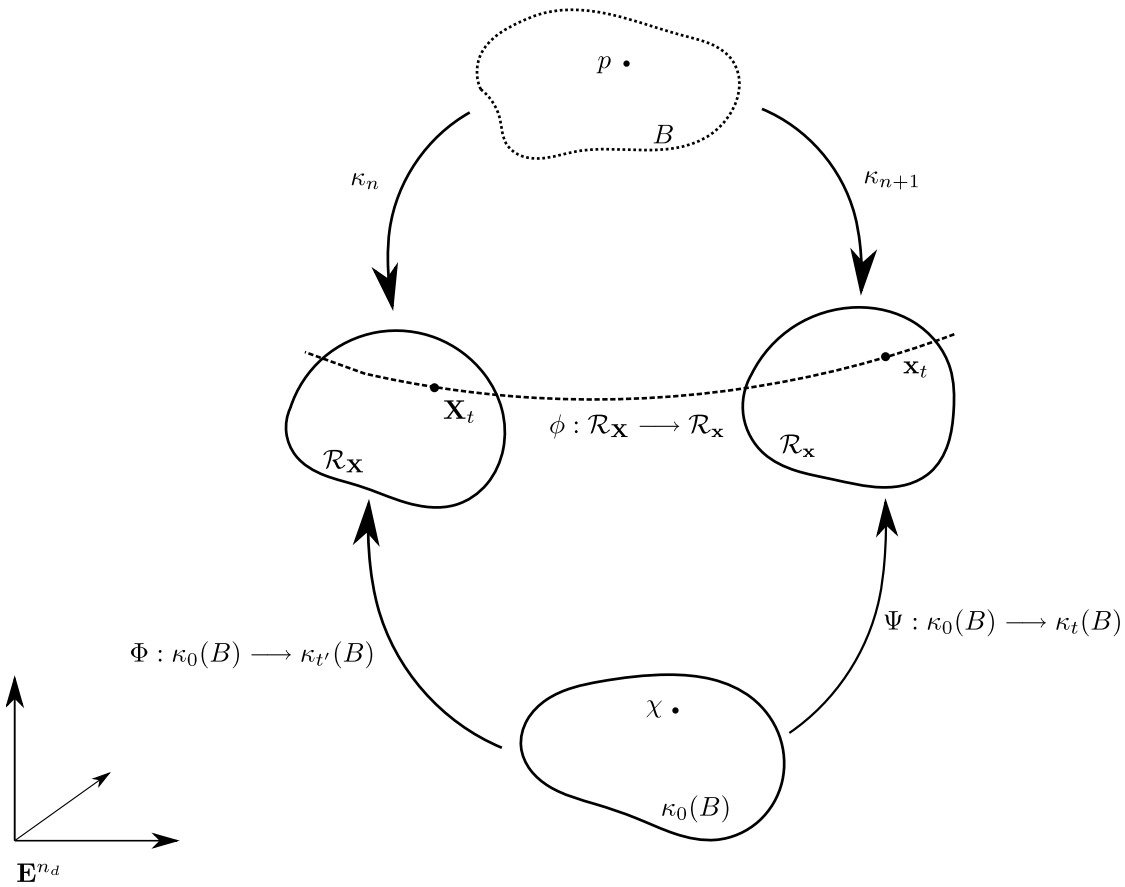

Figure 3.1.2: Material, spatial, and referential configurations.

We can furthermore define the gradient of the displacement in terms of the referential configuration as

$$\nabla_{\boldsymbol{\chi}}\mathbf{u}(\boldsymbol{\chi},t) \equiv \nabla_{\boldsymbol{\chi}}\Phi(\boldsymbol{\chi},t) - \nabla_{\boldsymbol{\chi}}\Psi(\boldsymbol{\chi},t). \tag{3.9}$$

For our purposes, the referential coordinates $\boldsymbol{\chi}$ will be describing the coordinates of a fixed FEM mesh.

Similar to the displacement field, we can describe the physical velocity field through the referential configuration as

$$\begin{aligned}
\mathbf{v}(\boldsymbol{\chi},t) &:= \frac{d\Phi(\Psi^{-1}(\mathbf{X},t),t)}{dt} && (3.10)\\
&= \frac{\partial\Phi(\boldsymbol{\chi},t)}{\partial t} + \frac{\partial\Phi(\boldsymbol{\chi},t)}{\partial\Psi^{-1}(\mathbf{X},t)}\frac{\partial\Psi^{-1}(\mathbf{X},t)}{\partial t} && (3.11)\\
&= \hat{\mathbf{v}} + \mathbf{w}\cdot\nabla_{\boldsymbol{\chi}}\mathbf{x} && (3.12)
\end{aligned}$$

where $\hat{\mathbf{v}} := \frac{\partial\mathbf{x}}{\partial t}\Big|_{\boldsymbol{\chi}}$ is the velocity of the reference configuration (mesh velocity in the context of FEM), and $\mathbf{w} := \frac{\partial\boldsymbol{\chi}}{\partial t}\Big|_{\mathbf{X}}$ is interpreted as the material velocity defined over the referential configuration.

Similarly, we can express the physical acceleration of a material particle through the referential configuration as

$$\begin{aligned}
\mathbf{a}(\boldsymbol{\chi},t) &:= \frac{d^2\mathbf{u}(\boldsymbol{\chi},t)}{d\,t^2} && (3.13)\\
&= \frac{\partial^2\mathbf{x}}{\partial t^2}\Big|_{\boldsymbol{\chi}} + \frac{\partial\mathbf{x}}{\partial\boldsymbol{\chi}}\frac{\partial^2\boldsymbol{\chi}}{\partial t^2}\Big|_{\mathbf{X}} && (3.14)
\end{aligned}$$

Alternatively we can express the physical acceleration by differentiating the velocity $\mathbf{v}(\boldsymbol{\chi},t)$:

$$\begin{aligned}
\mathbf{a}(\boldsymbol{\chi},t) &= \frac{d\mathbf{v}(\boldsymbol{\chi},t)}{dt} && (3.15)\\
&= \frac{\partial\mathbf{v}}{\partial t}\Big|_{\boldsymbol{\chi}} + \frac{\partial\mathbf{v}}{\partial\boldsymbol{\chi}}\frac{\partial\boldsymbol{\chi}}{\partial t}\Big|_{\mathbf{X}} && (3.16)\\
&= \frac{\partial\mathbf{v}}{\partial t}\Big|_{\boldsymbol{\chi}} + \mathbf{w}\cdot\nabla_{\boldsymbol{\chi}}\mathbf{v} && (3.17)
\end{aligned}$$

We can re-express above expression such that no spatial gradients with respect to the referential configurations need to be evaluated. We can achieve this by expressing the physical velocity in terms of spatial configuration:

$$\mathbf{a}(\boldsymbol{\chi}, t) = \frac{\partial \mathbf{v}}{\partial t}\Big|_{\boldsymbol{\chi}} + \frac{\partial \mathbf{v}}{\partial \mathbf{x}} \frac{\partial \mathbf{x}}{\partial \boldsymbol{\chi}} \frac{\partial \boldsymbol{\chi}}{\partial t}\Big|_{\mathbf{X}} \tag{3.18}$$

$$= \frac{\partial \mathbf{v}}{\partial t}\Big|_{\boldsymbol{\chi}} + \frac{\partial \mathbf{v}}{\partial \mathbf{x}} \left(\mathbf{v}(\boldsymbol{\chi}, t) - \hat{\mathbf{v}}(\mathbf{x}, t)\right) \tag{3.19}$$

$$= \frac{\partial \mathbf{v}}{\partial t}\Big|_{\boldsymbol{\chi}} + \mathbf{c} \cdot \nabla_{\mathbf{x}} \mathbf{v} \tag{3.20}$$

3.3 Deformation gradient, strain, and stress measures

Introduce the deformation gradient $\mathbf{F}$ as

$$\mathbf{F} := \frac{d\mathbf{x}}{d\mathbf{X}}, \tag{3.21}$$

and let $J := \det(\mathbf{F}) > 0$ be the determinant of the deformation gradient. The the Left and Right Cauchy-Green deformation tensors $\mathbf{C}$ and $\mathbf{B}$, respectively, are defined through the deformation gradient as

$$\mathbf{C} := \mathbf{F}^T \mathbf{F} \tag{3.22}$$

$$\mathbf{B} := \mathbf{F}\mathbf{F}^T. \tag{3.23}$$

With these in hand, we can define the nonlinear St. Venant strain tensor frequently which will be used for writing the constitutive equation as

$$\mathbf{E} := \frac{1}{2}\left(\mathbf{C} - \mathbf{I}\right), \tag{3.24}$$

and we note that the strain measure vanishes identically for a rigidly imposed deformation, making it suitable for use in problems where a body is subjected to large deformation.

The conservation laws are naturally written in terms of the Cauchy stress tensor $\boldsymbol{\tau}$ in the current configuration $R_{\mathbf{x}}$ which is not known *a priori*. At times, it is more convenient to use the refer to the second Piola-Kirchhoff stress $\mathbf{S}$ tensor which gives the stress measure in the reference configuration. We have

$$\boldsymbol{\tau} = \frac{1}{J}\mathbf{F}\mathbf{S}\mathbf{F}^T. \tag{3.25}$$

3.4 Conservation Laws

Resorting to a referential configuration, equations corresponding to the conservation of a (linear) momentum and mass for a continua written in non-conservative form become

$$\rho(\mathbf{x})\left(\frac{\partial \mathbf{v}}{\partial t}\Big|_{\boldsymbol{\chi}} + \mathbf{c}(\mathbf{x},t)\cdot\nabla_{\mathbf{x}}\mathbf{v}\right) = \nabla_{\mathbf{x}}\cdot\boldsymbol{\tau} + \mathbf{f}(\mathbf{x},t), \tag{3.26}$$

$$\frac{\partial \rho}{\partial t}\Big|_{\boldsymbol{\chi}} + \mathbf{c}(\mathbf{x},t)\cdot\nabla_{\mathbf{x}}\rho + \rho\nabla_{\mathbf{x}}\cdot\mathbf{v} = 0. \tag{3.27}$$

where, $\mathbf{v}$ is the velocity field of the body, $\mathbf{c}$ is the convective velocity field, $\boldsymbol{\tau}$ is the Cauchy stress tensor, ρ is the mass density, and $\mathbf{f}$ is the body force per unit volume.

The complete IBVP will be stated for fluid and the solid in the following sections.

4 Fluid

In this section, we will limit our discussion only to incompressible flows.

4.1 The IBVP

The IBVP for the fluid reads: Find $\mathbf{v} : \mathcal{R}_{\mathbf{x}} \times [0,T] \to \mathbb{E}^{n_d}$, $p : \mathcal{R}_{\mathbf{x}} \times [0,T] \to \mathbb{E}$ such that

$$\mathbf{r}_m := \rho\left(\frac{\partial \mathbf{v}}{\partial t}\Big|_{\boldsymbol{\chi}} + \mathbf{c}\cdot\nabla_{\mathbf{x}}\mathbf{v}\right) - \nabla_{\mathbf{x}}\cdot\boldsymbol{\tau} - \mathbf{f} = \mathbf{0}, \quad \text{in} \quad \mathcal{R}_{\mathbf{x}} \times [0,T], \tag{4.1}$$

$$r_d := \nabla_{\mathbf{x}}\cdot\mathbf{v} = 0 \quad \text{in} \quad \mathcal{R}_{\mathbf{x}} \times [0,T], \tag{4.2}$$

$$\mathbf{v} = \mathbf{g} \quad \text{in} \quad \Gamma_d \tag{4.3}$$

$$\boldsymbol{\tau}\cdot\mathbf{n} = \mathbf{t} \quad \text{in} \quad \Gamma_t \tag{4.4}$$

$$\mathbf{v} = \mathbf{v}_0 \quad \text{in} \quad \mathcal{R}_{\mathbf{x}} \times 0 \tag{4.5}$$

$$\dot{\mathbf{v}} = \dot{\mathbf{v}}_0 \quad \text{in} \quad \mathcal{R}_{\mathbf{x}} \times 0 \tag{4.6}$$

Remarks:

1. We have chosen to work with the Navier-Stokes equations written in a non-conservative form.

2. We will restrict our discussion to Newtonian fluids, for which we use the following constitutive equation:

$$\boldsymbol{\tau} = 2\mu\dot{\boldsymbol{\epsilon}} - \left(\frac{2}{3}\mu\,\mathrm{tr}(\dot{\boldsymbol{\epsilon}})\,\mathbf{I} + p\,\mathbf{I}\right), \tag{4.7}$$

   where, $\dot{\boldsymbol{\epsilon}} = \nabla_{\mathbf{x}}{}^{s}\mathbf{v} = \frac{1}{2}\left(\nabla_{\mathbf{x}}\mathbf{v} + \nabla_{\mathbf{x}}\mathbf{v}^{T}\right)$ is the (total) strain-rate tensor, μ is the kinematic viscosity of the fluid, and $\mathbf{I}$ is the identity tensor. Note that the first term in brackets of the constitutive equation vanishes for incompressible fluids. Since the incompressibility condition will be imposed in an average sense within the context of GFEM, we choose to retain this term.

3. If $\boldsymbol{\chi} \equiv \mathbf{x}$, we recover the Eulerian description of the flow, and if $\boldsymbol{\chi} \equiv \mathbf{X}$, we recover the Lagrangian description of the flow. Along the fluid-structure interface, the latter case holds.

4.2 Semi-discrete SUPG/PSPG stabilized ALE formulation

Two sources of difficulties arise when using standard Galerkin finite element method (GFEM) for solving the incompressible Navier-Stokes equations:

1. Spurious oscillations or "wiggles" in the numerical solution: For advection-dominated flows, and FEM meshes which under-resolve the gradient of the solution, the numerical solution exhibits spurious oscillations about the exact solutions. These oscillations can be avoided if the mesh is refined in regions where the solution exhibits a large gradient.

2. LBB condition in incompressible flows: for inadequately chosen solution spaces for pressure, existence of a solution to the discretized GFEM equations is not guaranteed.

See for instance [5] for an in-depth discussion regarding the two issues. In this context, we have adopted the Streamline Upwind Petrov-Galerkin (SUPG) method for stabilizing the convective terms, and adopted the Pressure Stabilizing Petrov-Galerkin (PSPG) for circumventing the LBB condition. In both of these methods, the Galerkin formulation Navier-Stokes equations is supplemented with the residual of the momentum equations.

The SUPG and PSPG formulation read (see [8]): find $\mathbf{v}^h \in S^h_{\mathbf{u}}$ and $p^h \in S^h_p$ such that

$$\begin{aligned}
\Big(\mathbf{w}^h\ ,\ \rho\frac{\partial \mathbf{v}^h(\boldsymbol{\chi},t)}{\partial t}\Big)_\Omega + \Big(\mathbf{w}^h\ ,\ \rho\mathbf{c}^h\cdot\nabla_{\mathbf{x}}\mathbf{v}^h\Big)_\Omega + \Big(\nabla_{\mathbf{x}}\mathbf{w}^h\ ,\ 2\mu\,\dot{\boldsymbol{\epsilon}}^h\Big)_\Omega \\
-\Big(\nabla_{\mathbf{x}}\mathbf{w}^h\ ,\ \frac{2}{3}\mu\,\mathrm{tr}(\dot{\boldsymbol{\epsilon}})\mathbf{I}\Big)_\Omega - \Big(\nabla_{\mathbf{x}}\mathbf{w}^h\ ,\ p^h\mathbf{I}\Big)_\Omega + \Big(\hat{\mathbf{w}}^h\ ,\ \mathbf{r}^h_m\Big)_\Omega = \Big(\mathbf{w}^h\ ,\ \mathbf{f}\Big)_\Omega \\
+\big\langle\mathbf{w}^h\ ,\ \mathbf{t}\big\rangle_{\Gamma_t} + \big\langle\mathbf{w}^h\ ,\ g\big\rangle_{\Gamma_d}, \qquad (4.8)
\end{aligned}$$

$$\Big(q^h\ ,\ \nabla_{\mathbf{x}}\cdot\mathbf{v}\Big)_\Omega + \Big(\hat{\mathbf{q}}^h\ ,\ \mathbf{r}^h_m\Big)_\Omega = 0 \qquad (4.9)$$

for all $\mathbf{w}^h \in \mathcal{V}^h_{\mathbf{v}}$ and $q \in \mathcal{V}^h_p$. In above equations, the last inner product on the left-hand-side is the residual of the momentum equations. The function spaces are defined as

$$\mathcal{S}^h_{v_i} = \{v^h_i | v^h_i \in H^{1h}(\Omega), v^h_i = g^h_i \text{ on } \Gamma_g\}, \qquad (4.10)$$

$$\mathcal{V}_{u_i} = \{w^h_i | w^h_i \in H^{1h}(\Omega), w^h_i = 0 \text{ on } \Gamma_g\}, \qquad (4.11)$$

$$\mathcal{S}_p = V^h_p = \{q^h | q^h \in H^{1h}(\Omega)\}. \qquad (4.12)$$

Note that within this formulation, as discussed in Section 2.1, GCL is automatically satisfied regardless of the movement of mesh.

4.3 Solution strategy

From this point on, we consider the matrix form of the above discretized equations written as.

$$\bar{\mathbf{M}}_m\mathbf{a} + \big[\bar{\mathbf{K}}_m + \bar{\mathbf{A}}_m(\mathbf{c})\big]\,\mathbf{v} - \bar{\mathbf{G}}_m\mathbf{p} = \bar{\mathbf{F}}_m, \qquad (4.13)$$

$$\bar{\mathbf{M}}_c\mathbf{a} + \big[\mathbf{G}^T + \bar{\mathbf{K}}_c + \bar{\mathbf{A}}_c(\mathbf{c})\big]\,\mathbf{v} + \mathbf{L}\mathbf{p} = \mathbf{F}_c, \qquad (4.14)$$

where,

$$\bar{\mathbf{M}}_m^{ij} = \rho \int_\Omega \left(\mathbf{N} + \hat{\mathbf{N}}_{SUPG}\right) \mathbf{N}^T \, d\mathbf{x} \, \delta_{ij}, \tag{4.15}$$

$$\bar{\mathbf{A}}_m^{ij}(\mathbf{u}) = \rho \int_\Omega \left(\mathbf{N} + \hat{\mathbf{N}}_{SUPG}\right) \mathbf{c} \cdot \nabla_{\mathbf{x}} \mathbf{N}^T \, d\mathbf{x} \, \delta_{ij}, \tag{4.16}$$

$$\bar{\mathbf{K}}_m = \mathbf{K} + \mathbf{K}_{SUPG}, \tag{4.17}$$

$$\mathbf{K}^{ij} = \mu \int_\Omega \nabla_{\mathbf{x}} \mathbf{N} \cdot \nabla_{\mathbf{x}} \mathbf{N}^T \, d\mathbf{x} \, \delta_{ij} + \mu \int_\Omega \mathbf{N}_{,j} \, \mathbf{N}_{,i}^T \, d\mathbf{x} - \frac{2}{3}\mu \int_\Omega \mathbf{N}_{,i} \mathbf{N}_{,j}^T \, d\mathbf{x} \, \delta_{ij}, \tag{4.18}$$

$$\mathbf{K}_{SUPG}^{ij} = \mu \int_\Omega \hat{\mathbf{N}}_{SUPG} \mathbf{N}_{,kk}^T \, d\mathbf{x} \, \delta_{ij} + \mu \int_\Omega \hat{\mathbf{N}}_{SUPG} \left(\mathbf{N}_{,ji}^T - \frac{2}{3}\mathbf{N}_{,ij}^T\right) \, d\mathbf{x} \tag{4.19}$$

$$\mathbf{G}^i = \int_\Omega \mathbf{N}_{,i} \, \mathbf{N}^T \, d\mathbf{x}, \tag{4.20}$$

$$\bar{\mathbf{G}}_m^i = \int_\Omega \left(\mathbf{N}_{,i} \, \mathbf{N}^T - \hat{\mathbf{N}}_{SUPG} \mathbf{N}_{,i}^T\right) \, d\mathbf{x}, \tag{4.21}$$

$$\bar{\mathbf{F}}_m^i = \int_\Omega \left(\mathbf{N} + \hat{\mathbf{N}}_{SUPG}\right) f_i \, d\mathbf{x} + \int_{\partial\Omega} \mathbf{N} \, \tau_{ij}^h n_j \, d\mathbf{s}, \tag{4.22}$$

$$\bar{\mathbf{M}}_c^{ij} = \rho \int_\Omega \hat{\mathbf{N}}_{PSPG} \, \mathbf{N}^T \, d\mathbf{x} \, \delta_{ij}, \tag{4.23}$$

$$\bar{\mathbf{A}}_c^{ij}(\mathbf{u}) = \rho \int_\Omega \hat{\mathbf{N}}_{PSPG} \, \mathbf{c} \cdot \nabla_{\mathbf{x}} \mathbf{N}^T \, d\mathbf{x} \, \delta_{ij}, \tag{4.24}$$

$$\mathbf{L} = \int_\Omega \nabla_{\mathbf{x}} \hat{\mathbf{N}}_{PSPG} \cdot \nabla_{\mathbf{x}} \mathbf{N}^T \, d\mathbf{x}, \tag{4.25}$$

$$\mathbf{F}_c^i = \int_\Omega \hat{\mathbf{N}}_{PSPG} \, f_i \, d\mathbf{x}. \tag{4.26}$$

In above, the augmented shape functions $\hat{\mathbf{N}}_{SUPG}$ and $\hat{\mathbf{N}}_{PSPG}$ are given by

$$\hat{\mathbf{N}}_{SUPG} = \tau_{SUPG} \left(\mathbf{c} \cdot \nabla_{\mathbf{x}} \mathbf{N}\right), \tag{4.27}$$

$$\hat{\mathbf{N}}_{PSPG} = \frac{\tau_{PSPG}}{\rho} \nabla_{\mathbf{x}} \mathbf{N}. \tag{4.28}$$

In above, matrices $\mathbf{M}$, $\mathbf{K}$, $\mathbf{A}$, and $\mathbf{G}$ are contributions from the inertia, viscous, advection, and pressure terms, respectively, and τ_{SUPG} and τ_{PSPG} are stabilization parameters (not to be confused with the stress tensor $\boldsymbol{\tau}$). Note that GFEM form of the equations is obtained by letting $\tau_{SUPG} = \tau_{PSPG} = 0$.

The success of the stabilized methods relies on the choice of the stabilization parameters τ_{SUPG} and τ_{PSPG}. In this work, we have taken values suggested by [8], summarized below:

$$\tau_{SUPG} := \frac{h}{2||\mathbf{v}^h||} z(Re_{\text{SUPG}}), \tag{4.29}$$

$$\tau_{PSPG} := \frac{h^{\#}}{2||\mathbf{V}||} z(Re_{\text{PSPG}}), \tag{4.30}$$

$$z(Re) := \begin{cases} Re/3, & 0 \leq Re \leq 3 \\ 1, & 3 \leq Re \end{cases} \tag{4.31}$$

where the "element Reynold numbers" Re are defined as

$$Re_{\text{SUPG}} := \rho \frac{||\mathbf{v}^h|| h_{\text{SUPG}}}{2\mu}, \tag{4.32}$$

$$Re_{\text{PSPG}} := \rho \frac{||\mathbf{V}^h|| h_{\text{PSPG}}}{2\mu}, \tag{4.33}$$

where,

$$h_{\text{SUPG}} := 2 \left(\sum_{a=1}^{n_{en}} |\mathbf{s} \cdot \nabla_{\mathbf{x}} N_a| \right)^{-1}, \tag{4.34}$$

$$h_{\text{PSPG}} := 2\sqrt{\frac{A_e}{\pi}}, \tag{4.35}$$

and $\mathbf{s}$ is the unit vector in the direction of the local velocity, $\mathbf{N}_a$ is the basis function associated with node a, n_{en} is the number of nodes in an element, and A_e is the area of an element.

Note that $\tau = \mathcal{O}(h)$ for advection dominated flows, while $\tau = \mathcal{O}(h^2)$ for convection dominated flows. Some of the alternative proposed forms for stabilization parameters, for instance those given in [6], take on a simpler form, but are of order h for all flow types and can result in degradation of the accuracy of the numerical scheme.

We have here considered the semi-discrete scheme, and the continuity of the solution in time is enforced through a finite differencing scheme. Employing the generalized trapezoidal scheme, we have

$$\mathbf{v}^{n+1} = \mathbf{v}^n + \Delta t \left[\theta \mathbf{a}^{n+1} + (1-\theta) \mathbf{a}^n \right], \tag{4.36}$$

where $\theta \in (0, 1]$ determines the accuracy and stability of the time integration scheme. Note that the choice of $\theta = 1/2$ results in the second-order accurate Crank-Nicolson scheme, while $\theta = 1$ results in the first-order accurate implicit-Euler scheme.

Above equations represent a coupled set of nonlinear equations. The nonlinearity is due to the presence of the convection terms $\mathbf{c}$. In this context, we construct a Newton-Raphson iterative scheme for solving the nonlinear equations above.

Denote by $\mathcal{R}(\mathbf{U}^{i+1})$ the residual of the discretized equations at iteration $i+1$, where $\mathbf{U}$ is a vector containing the finite element unknowns (both $\mathbf{u}^h$ and p^h). Expanding the residual about iteration i using Taylor's formula gives

$$\mathcal{R}(\mathbf{U}^{i+1}) = \mathcal{R}(\mathbf{U}^i) + \frac{\partial \mathcal{R}}{\partial \mathbf{U}}\Big|_i \Delta\mathbf{U} + \mathcal{O}((\Delta\mathbf{U})^2) = 0, \tag{4.37}$$

where $\Delta\mathbf{U} = \mathbf{U}^{i+1} - \mathbf{U}^i$ is the difference between two successive iterations. Neglecting higher-order terms, the iterative scheme becomes

$$(\mathbf{U}^{i+1} - \mathbf{U}^i) = -\mathcal{J}^{-1}\left(\mathcal{R}(\mathbf{U}^i)\right), \tag{4.38}$$

where we have defined the Jacobian matrix as $\mathcal{J} := \frac{\partial \mathcal{R}}{\partial \mathbf{U}}$.

Expanded form of the iterative scheme which is more suitable for computations is given as

$$\begin{aligned}\left[\frac{1}{\theta\Delta t}\bar{\mathbf{M}}_m^i + (\bar{\mathbf{K}}_m^i + \bar{\mathbf{A}}_m^i) + \frac{\partial \bar{\mathbf{A}}_m^i}{\partial \mathbf{v}}\mathbf{v}^i\right]\Delta\mathbf{v}^{i+1} - \bar{\mathbf{G}}_m\Delta\mathbf{p}^{i+1} \\ = \bar{\mathbf{F}}_m - \left[\bar{\mathbf{M}}_m^i\mathbf{a}^i + \left(\bar{\mathbf{K}}_m^i + \bar{\mathbf{A}}_m^i\right)\mathbf{v}^i - \bar{\mathbf{G}}_m\mathbf{p}^i\right]\end{aligned} \tag{4.39}$$

$$\begin{aligned}\left[\frac{1}{\theta\Delta t}\bar{\mathbf{M}}_c^i + (\bar{\mathbf{G}}_c + \bar{\mathbf{K}}_c^i + \bar{\mathbf{A}}_c^i) + \frac{\partial \bar{\mathbf{A}}_c^i}{\partial \mathbf{v}}\mathbf{v}^i\right]\Delta\mathbf{v}^{i+1} + \mathbf{L}\,\Delta\mathbf{p}^{i+1} \\ = \bar{\mathbf{F}}_c - \left[\bar{\mathbf{M}}_c^i\mathbf{a}^i + \left(\bar{\mathbf{G}}_c + \bar{\mathbf{K}}_c^i + \bar{\mathbf{A}}_c^i\right)\mathbf{v}^i + \mathbf{L}\mathbf{p}^i\right]\end{aligned} \tag{4.40}$$

where superscripts n and i denote time-step n and iteration i, respectively.

5 Structure

It is convenient to cast the governing equations for the structure in their natural Lagrangian setting. The conservation law in the Lagrangian setting is obtained by setting $\Psi = id_{\mathbf{X}}$ ($\Rightarrow \boldsymbol{\chi} \equiv \mathbf{X}$), where $id_{\mathbf{X}}$ is the identity operator defined over $R_{\mathbf{X}}$. The resulting expression for the conservation of linear momentum in a Lagrangian takes the following simpler form of

$$\rho(\mathbf{x})\frac{\partial^2 \mathbf{u}}{\partial t^2}\Big|_{\boldsymbol{X}} = \nabla_{\mathbf{x}}\boldsymbol{\tau} + \mathbf{f}, \tag{5.1}$$

while the mass conservation is trivially satisfied in the Lagrangian framework.

We will limit our discussion to nonlinear elastic materials described by the Saint-Venant Kirchhoff material model given by

$$\boldsymbol{\tau} = \frac{1}{J}\mathbf{F}\left[\lambda^s \operatorname{tr}(\mathbf{E})\mathbf{I} + 2\mu^s\mathbf{E}\right]\mathbf{F}^T, \tag{5.2}$$

where λ^s and μ^s are Lamé constants, and $\mathbf{E}$ is the St. Venant strain tensor introduced in Section 3.3.

The complete IBVP corresponding to the balance of (angular) momentum written in the Lagrangian formulation stated as: Find $\mathbf{u} : \mathcal{R}_{\mathbf{x}} \times [0, T] \to \mathbb{E}^{n_d}$ such that

$$\rho(\mathbf{x})\frac{\partial^2 \mathbf{u}}{\partial t^2}\Big|_{\mathbf{X}} - \nabla_{\mathbf{x}} \cdot \boldsymbol{\tau} = \mathbf{f} \quad \text{in} \quad \mathcal{R}_{\mathbf{x}} \times [0, T], \tag{5.3}$$

$$\mathbf{u} = \mathbf{g} \quad \text{in} \quad \Gamma_d \tag{5.4}$$

$$\boldsymbol{\tau} \cdot \mathbf{n} = \mathbf{t} \quad \text{in} \quad \Gamma_t \tag{5.5}$$

$$\mathbf{u} = \mathbf{u}_0 \quad \text{in} \quad \mathcal{R}_{\mathbf{x}} \times 0 \tag{5.6}$$

$$\mathbf{v} = \mathbf{v}_0 \quad \text{in} \quad \mathcal{R}_{\mathbf{x}} \times 0 \tag{5.7}$$

where $\mathbf{u}$ and $\mathbf{u}_0$ are the displacement field and initial displacement field of the body, respectively, $\boldsymbol{\tau}$ is the Cauchy stress tensor, $\mathbf{f}$ is the body force per unit-volume, and $\mathbf{v}$ is the velocity field.

5.1 Variational Formulation

Introduce the weight function space $\mathcal{V} := \Big\{\hat{w}_i \,|\, \hat{w}_i \in H^1(\kappa_t(B)), \hat{w}_i = 0 \text{ on } \Gamma_d(\kappa_t(B))\Big\}$, and write

$$\big(\mathbf{w}\ ,\ \rho\,\mathbf{a}\big)_{\kappa_t(B)} + \big(\mathbf{w}, -\nabla_{\mathbf{x}}\cdot\boldsymbol{\tau}\big)_{\kappa_t(B)} = \big(\mathbf{w}, \mathbf{f}\big)_{\kappa_t(B)}. \tag{5.8}$$

Performing integration on parts on the stress divergence term yields

$$\big(\mathbf{w}\ ,\ \rho\,\mathbf{a}\big)_{\kappa_t(B)} + \big(\nabla_{\mathbf{x}}\mathbf{w}\ ,\ \boldsymbol{\tau}\big)_{\kappa_t(B)} = \big(\mathbf{w}\ ,\ \mathbf{f}\big)_{\kappa_t(B)} + \big\langle\mathbf{w}\ ,\ \mathbf{t}\big\rangle_{\Gamma_n(\kappa_t(B))}. \tag{5.9}$$

The second inner product can be evaluated over the material configuration by resorting to the use of the 2nd Piola-Kirchhoff's stress tensor $\mathbf{S}$:

$$\begin{aligned}\Big(\nabla_{\mathbf{x}}\mathbf{w}\ ,\ \boldsymbol{\tau}\Big)_{\kappa_t(B)} &= \Big(\nabla_{\mathbf{X}}\mathbf{w}\,\mathbf{F}^{-1}\ ,\ \frac{1}{J}\mathbf{F}\mathbf{S}\mathbf{F}^T\Big)_{\kappa_t(B)}\\ &= \Big(\nabla_{\mathbf{X}}\mathbf{w}\,\mathbf{F}^{-1}\ ,\ \mathbf{F}\mathbf{S}\mathbf{F}^T\Big)_{\kappa_0(B)}\\ &= \Big(\nabla_{\mathbf{X}}\mathbf{w}\ ,\ \mathbf{S} + \mathbf{S}\nabla_{\mathbf{X}}\mathbf{u}^T\Big)_{\kappa_0(B)}.\end{aligned} \tag{5.10}$$

The variational formulation is now complete and reads: Find $u_i \in \mathcal{S}$ such that

$$\Big(\mathbf{w}\ ,\ \rho\ddot{\mathbf{u}}\Big)_{\kappa_0(B)} + \Big(\nabla_{\mathbf{X}}\mathbf{w}\ ,\ \mathbf{S} + \mathbf{S}\nabla_{\mathbf{X}}\mathbf{u}^T\Big)_{\kappa_0(B)} \tag{5.11}$$

$$= \Big(\mathbf{w}\ ,\ \mathbf{f}\Big)_{\kappa_t(B)} + \big\langle\mathbf{w}\ ,\ \mathbf{t}\big\rangle_{\Gamma_t(\kappa_t(B))}, + \big\langle\mathbf{w}\ ,\ \mathbf{g}\big\rangle_{\Gamma_n(\kappa_t(B))}, \quad \forall\mathbf{w}\in\mathcal{V}. \tag{5.12}$$

Note that the right-hand-side of the above equation is evaluated over the reference configuration (including the gradients), and the left-hand-side is evaluated over the final configuration.

Hereon, we shall make the simplifying assumption that the body forces and the tractions are independent of the configuration of the body and evaluate the rhs of the equilibrium equations over the reference configuration.

5.2 Semi-Discrete Galerkin Method

Let the continuous solution $u_i(x,t)$ be approximated as

$$u_i^h(x,t) = \mathbf{N}^T(x)\mathbf{u}_i^h(t), \tag{5.13}$$

where $\mathbf{N}(x)$ is an array containing interpolation functions, and $u_i^h(t)$ is an array containing the discretized nodal values of $u_i^h(x,t)$. Finally, define the finite-dimensional trial function space

$$\mathcal{S}^h := \left\{ u_i^h(x,t) \,|\, u_i^h(x,t) \in H^1(\kappa_t(B)), u_i(x,t) = g_i \text{ on } \Gamma_d(\kappa_t(B)) \right\} \quad \forall t \in [0,T] \tag{5.14}$$

The semi-discrete Galerkin method becomes to find $u_i^h \in \mathcal{S}^h$ such that

$$\begin{aligned} \left(\mathbf{w}^h \,,\, \rho\ddot{\mathbf{u}}^h\right)_{\kappa_0(B)} + \left(\nabla_{\mathbf{X}}\mathbf{w}^h \,,\, \mathbf{S}^h + \mathbf{S}^h\nabla_{\mathbf{X}}(\mathbf{u}^h)^T\right)_{\kappa_0(B)} \\ = \left(\mathbf{w}^h \,,\, \mathbf{f}^h\right)_{\kappa_t(B)} + \left\langle \mathbf{w}^h \,,\, \boldsymbol{\tau}^h \cdot \mathbf{n}\right\rangle_{\Gamma_n(\kappa_t(B))}, \quad \forall \mathbf{w}^h \in \mathcal{V}^h \end{aligned} \tag{5.15}$$

Owning to the symmetric operator, the GFEM formulation to the elasticity problem does not suffer from any spurious wiggles and no stabilization parameters are needed.

5.3 Solution procedure

The variational formulation in previous section can be nonlinear owning to the constitutive model employed. We aim to solve the resulting nonlinear equations using a Newton-Raphson iterative scheme as done in the case of the incompressible Navier-Stokes equations.

$$\begin{aligned} \frac{\partial}{\partial\ddot{\mathbf{u}}^h}\left(\mathbf{w}^h \,,\, \rho\ddot{\mathbf{u}}^h\right)_{\kappa_0(B)}\Delta\ddot{\mathbf{u}}^h + \frac{\partial}{\partial\mathbf{u}^h}\left(\nabla_{\mathbf{X}}\mathbf{w}^h \,,\, \mathbf{S}^{h,i} + \mathbf{S}^{h,i}\nabla_{\mathbf{X}}(\mathbf{u}^{h,i})^T\right)_{\kappa_0(B)}\Delta\ddot{\mathbf{u}} \\ = \left(\mathbf{w}^h \,,\, \mathbf{f}^h\right)_{\kappa_t(B)} + \left\langle \mathbf{w}^h \,,\, \boldsymbol{\tau}^h \cdot \mathbf{n}\right\rangle_{\Gamma_n(\kappa_t(B))} - \left(\mathbf{w}^h \,,\, \rho\ddot{\mathbf{u}}^{h,i}\right)_{\kappa_0(B)} \\ -\left(\nabla_{\mathbf{X}}\mathbf{w}^h \,,\, \mathbf{S}^{h,i} + \mathbf{S}^{h,i}\nabla_{\mathbf{X}}(\mathbf{u}^{h,i})^T\right)_{\kappa_0(B)} \end{aligned} \tag{5.16}$$

Components of the above expression can be re-written as follows:

$$\left(\nabla_{\mathbf{X}}\mathbf{w}^h\ ,\ \mathbf{S}^h + \mathbf{S}^h\nabla_{\mathbf{X}}(\mathbf{u}^h)^T\right)_{\kappa_0(B)} = \left(\mathbf{w}^h\ ,\ (\mathbf{B}_L + \mathbf{B}_{NL})\{\mathbf{S}^h\}\right)_{\kappa_0(B)} \tag{5.17}$$

$$\begin{aligned}
\frac{\partial}{\partial \mathbf{u}^h}\left(\nabla_{\mathbf{X}}\mathbf{w}^h\ ,\ \mathbf{S}^{h,i} + \mathbf{S}^{h,i}\nabla_{\mathbf{X}}(\mathbf{u}^{h,i})^T\right)_{\kappa_0(B)} &= \frac{\partial}{\partial \mathbf{u}^h}\left(\nabla_{\mathbf{X}}\mathbf{w}^h\ ,\ \mathbf{S}^h\right)_{\kappa_0(B)} \\
&\quad + \left(\nabla_{\mathbf{X}}\mathbf{w}^h\ ,\ \frac{\partial \mathbf{S}^h}{\partial \mathbf{u}^h}\nabla_{\mathbf{X}}(\mathbf{u}^h)^T\right)_{\kappa_0(B)} \\
&\quad + \left(\nabla_{\mathbf{X}}\mathbf{w}^h\ ,\ \mathbf{S}^h\frac{\partial}{\partial \mathbf{u}^h}(\nabla_{\mathbf{X}}\mathbf{u}^h)^T\right)_{\kappa_0(B)} \qquad (5.18) \\
&= (\mathbf{B}_L + \mathbf{B}_{NL})^T\mathbf{D}(\mathbf{B}_L + \mathbf{B}_{NL}) \\
&\quad + \hat{\mathbf{B}}^T\hat{\mathbf{S}}\hat{\mathbf{B}} \qquad (5.19)
\end{aligned}$$

Rearranging, the above set of equations can be cast in a more compact matrix form

$$\mathbf{M}\ddot{\mathbf{u}} + \mathbf{K}\Delta\mathbf{u} = \mathbf{F}, \tag{5.20}$$

where,

$$\mathbf{M}^{ij} = \rho\int_\Omega \mathbf{N}\mathbf{N}^T\,d\mathbf{x} \tag{5.21}$$

$$\mathbf{K} = \int_\Omega (\mathbf{B}_L + \mathbf{B}_{NL})^T\,\mathbf{D}\,(\mathbf{B}_L + \mathbf{B}_{NL})\ d\mathbf{X} + \int_\Omega \hat{\mathbf{B}}^T\hat{\mathbf{S}}\hat{\mathbf{B}}\,d\mathbf{X} \tag{5.22}$$

$$\begin{aligned}
\mathbf{F} &= \int_\Omega \mathbf{N}\mathbf{f}\,d\mathbf{x} - \int_\Omega (\mathbf{B}_L + \mathbf{B}_{NL})^T\{\mathbf{S}\}\,d\mathbf{X} \\
&\quad + \int_{\partial\Omega_n}\mathbf{N}\mathbf{t}\,d\mathbf{x} + \int_{\partial\Omega_d}\mathbf{N}\mathbf{g}\,d\mathbf{x} \qquad (5.23)
\end{aligned}$$

where,

$$\mathbf{B}_L = \begin{pmatrix} \mathbf{N}_{,1}^T & \mathbf{0} \\ \mathbf{0} & \mathbf{N}_{,2}^T \\ \mathbf{N}_{,2}^T & \mathbf{N}_{,1}^T \end{pmatrix}, \tag{5.24}$$

$$\mathbf{B}_{NL} = \begin{pmatrix} u_{1,1}\mathbf{N}_{,1}^T & u_{2,1}\mathbf{N}_{,1}^T \\ u_{1,2}\mathbf{N}_{,2}^T & u_{2,2}\mathbf{N}_{,2}^T \\ u_{1,1}\mathbf{N}_{,2}^T + u_{1,2}\mathbf{N}_{,1}^T & u_{2,1}\mathbf{N}_{,2}^T + u_{2,2}\mathbf{N}_{,1}^T \end{pmatrix}, \tag{5.25}$$

$$\{\mathbf{S}\} = \begin{pmatrix} S_{11} \\ S_{22} \\ S_{12} \end{pmatrix}, \tag{5.26}$$

$$\hat{\mathbf{B}} = \begin{pmatrix} \mathbf{N}_{,1}^T & \mathbf{0} \\ \mathbf{N}_{,2}^T & \mathbf{0} \\ \mathbf{0} & \mathbf{N}_{,1}^T \\ \mathbf{0} & \mathbf{N}_{,2}^T \end{pmatrix}, \tag{5.27}$$

$$\hat{\mathbf{S}} = \left(\begin{array}{c|c} \mathbf{S} & \mathbf{0} \\ \hline \mathbf{0} & \mathbf{S} \end{array}\right), \tag{5.28}$$

$$\mathbf{D}_{\text{strain}} = \frac{E}{(1+\nu)(1-2\nu)} \begin{pmatrix} 1-\nu & \nu & 0 \\ \nu & 1-\nu & 0 \\ 0 & 0 & \frac{1-2\nu}{2} \end{pmatrix} \tag{5.29}$$

$$\mathbf{D}_{\text{stress}} = \frac{E}{1-\nu^2} \begin{pmatrix} 1 & \nu & 0 \\ \nu & 1 & 0 \\ 0 & 0 & \frac{1-\nu}{2} \end{pmatrix} \tag{5.30}$$

and $\mathbf{D}$ is a constitutive matrix.

As in the case of the fluid formulation, above equations are have been obtained using a semi-discrete method. The continuity of the solution in time is enforced using finite differencing. More specifically, the acceleration is approximated using a generalized trapezoidal rule while the velocity approximation is evaluated using Newmark β-scheme:

$$\mathbf{v}^{n+1} = \mathbf{v}^n + \Delta t \left[\theta \mathbf{a}^{n+1} + (1-\theta)\mathbf{a}^n\right], \tag{5.31}$$

$$\mathbf{u}^{n+1} = \mathbf{u}^n + \mathbf{v}^n \Delta t + \left[\left(\frac{1}{2} - \beta\right)\mathbf{a}^n + \beta \mathbf{a}^{n+1}\right](\Delta t)^2. \tag{5.32}$$

In above, β and θ determine the accuracy and stability of the scheme. Note that the choice of $\theta = \frac{1}{2}$ and $\beta = \frac{1}{4}$ results in the the 'constant average acceleration method'

(Crank-Nicolson), while the choice of $\theta = \frac{1}{2}$ and $\beta = \frac{1}{6}$ results in the so-called 'linear acceleration method'. Using these equations, we can express the accelerations in the final configuration in terms of the displacements, velocities, and accelerations from the previous configuration, and also the estimate of displacements for the current configurations:

$$\mathbf{a}^{n+1} = \frac{1}{\beta \Delta t^2}(\mathbf{u}^{n+1} - \mathbf{u}^n) - \frac{1}{\beta \Delta t}\mathbf{v}^n + \left(1 - \frac{1}{2\beta}\right)\mathbf{a}^n. \tag{5.33}$$

Therefore, the iterative scheme using the Newton-Raphson scheme becomes

$$\begin{aligned}\left(\frac{1}{\beta \Delta t^2}\mathbf{M} + \mathbf{K}^i\right)\Delta \mathbf{u} &= \mathbf{F}^{n+1} \\ &\quad - \mathbf{M}^i\left[\frac{1}{\beta \Delta t^2}(\mathbf{u}^i - \mathbf{u}^n) - \frac{1}{\beta \Delta t}\mathbf{v}^n + \left(1 - \frac{1}{2\beta}\right)\mathbf{a}^n\right].\end{aligned} \tag{5.34}$$

6 Monolithic approach

In order to distinguish between the state variables, we use subscripts f, s, and m to distinguish state variables defined over the fluid, the solid, and the mesh domain, respectively. Variables $\mathbf{u}$, $\mathbf{v}$ and $\mathbf{a}$ are reserved to describe displacement, velocity, and acceleration fields. For instance, $\mathbf{v}_f$ denotes the velocity field in the fluid, $\mathbf{v}_s$ denotes the velocity field defined over the solid, and $\mathbf{v}_m$ denotes the velocity field of the computational mesh.

The discretized equations corresponding to the governing equations for the fluid and the mesh dynamics are summarized as follows:

Fluid:

$$\left[\frac{1}{\theta\Delta t}\bar{\mathbf{M}}_m^i + (\bar{\mathbf{K}}_m^i + \bar{\mathbf{A}}_m^i) + \frac{\partial\bar{\mathbf{A}}_m^i}{\partial\mathbf{v}}\mathbf{v}^i\right]\Delta\mathbf{v}^{i+1} + \frac{\partial\bar{\mathbf{A}}_m^i}{\partial\mathbf{w}}\mathbf{v}^i\Delta\mathbf{w}^{i+1} - \bar{\mathbf{G}}_m\Delta\mathbf{p}^{i+1} = \bar{\mathbf{F}}_m - \left[\bar{\mathbf{M}}_m^i\mathbf{a}^i + \left(\bar{\mathbf{K}}_m^i + \bar{\mathbf{A}}_m^i\right)\mathbf{v}^i - \bar{\mathbf{G}}_m\mathbf{p}^i\right] \tag{6.1}$$

$$\left[\frac{1}{\theta\Delta t}\bar{\mathbf{M}}_c^i + (\bar{\mathbf{G}}_c + \bar{\mathbf{K}}_c^i + \bar{\mathbf{A}}_c^i) + \frac{\partial\bar{\mathbf{A}}_c^i}{\partial\mathbf{v}}\mathbf{v}^i\right]\Delta\mathbf{v}^{i+1} + \frac{\partial\bar{\mathbf{A}}_c^i}{\partial\mathbf{w}}\Delta\mathbf{w}^i + \mathbf{L}\,\Delta\mathbf{p}^{i+1} = \bar{\mathbf{F}}_c - \left[\bar{\mathbf{M}}_c^i\mathbf{a}^i + \left(\bar{\mathbf{G}}_c + \bar{\mathbf{K}}_c^i + \bar{\mathbf{A}}_c^i\right)\mathbf{v}^i + \mathbf{L}\mathbf{p}^i\right] \tag{6.2}$$

Solid:

$$\left(\frac{1}{\beta\Delta t^2}\mathbf{M} + \mathbf{K}^i\right)(\mathbf{u}^{i+1} - \mathbf{u}^i) = \mathbf{F}^{n+1} - \mathbf{M}^i\left[\frac{1}{\beta\Delta t^2}(\mathbf{u}^i - \mathbf{u}^n) - \frac{1}{\beta\Delta t}\mathbf{v}^n + \left(1 - \frac{1}{2\beta}\mathbf{a}^n\right)\right]. \tag{6.3}$$

Mesh algorithm:

$$\mathbf{K}_m\Delta\mathbf{u}_m = \mathbf{F}_m - \mathbf{K}_m\mathbf{u}_m^i \tag{6.4}$$

Equation (6.4) describes a general set of equations for updating the configuration of the computational domain under prescribed displacements of the solid domain. Currently, the mesh movement is accommodated by solving the linearized elasticity equations.

6.1 Coupling

Coupling between the different domains are achieved through the equations at the interface between the fluid and the solid are continuity velocities and continuity of tractions. When using conforming elements at the interface, the latter (balance of tractions) can be replaced by the requiring balance of forces at the interface. These two equations can be written as

$$-\mathbf{v}_f + \mathbf{v}_s = \mathbf{0}, \tag{6.5}$$

$$-\mathbf{F}_f + \mathbf{F}_s = \mathbf{0}. \tag{6.6}$$

Enforcement of continuity of velocities across the fluid-structure interface is established through interface elements. Since $\mathbf{v}_s$ does not appear as a state variable, we enforce the discretized equation using the previously described one-step θ-scheme:

$$-\Delta\mathbf{v}_f + \frac{1}{\theta\Delta t}\Delta\mathbf{u}_s = -\left(-\mathbf{v}_f + \frac{1}{\theta\Delta t}(\mathbf{u}_s^i - \mathbf{u}_s^n) + \frac{\theta-1}{\theta}\mathbf{v}_s^n\right) \tag{6.7}$$

where $\theta \in (0, 1]$ was introduced before for temporal discretization of the fluid equations. Finally, the systems of Equations (6.1), (6.3), and (6.4) are augmented through Eq. (6.7). Similarly, the mesh algorithm is coupled by requiring that the fluid and the solid remain in contact for all t:

$$-\Delta\mathbf{u}_s + \Delta\mathbf{u}_m^i = -\left(\mathbf{u}_s^i - \mathbf{u}_m\right). \tag{6.8}$$

We further augment the state variables by introducing $\mathbf{F}_{\text{FSI}}$ as a state variable which is the common force at the interface between the fluid and the solid, and $\mathbf{F}_m$ as the common (fictitious) force between the solid and the mesh.

6.2 Structure of the final systems of equations

The final (nonlinear) systems of equations to be solved iteratively can be written in the form

$$\mathbf{A}(\mathbf{v}_f, \mathbf{u}_m, \mathbf{u}_s)\,\mathbf{y} = \mathbf{b}. \tag{6.9}$$

The structure of matrix $\mathbf{A}$ can be emphasized by writing above equation as

$$\left(\begin{array}{c|c|c|c|c|c}
\times & \times & & \otimes & \circ & \\ \hline
\times & \times & & \otimes & & \\ \hline
 & & \times & & \circ & \\ \hline
 & & & \circ & & \circ \\ \hline
\circ & & \circ & & & \\ \hline
 & & \circ & \circ & &
\end{array}\right)
\left(\begin{array}{c}
\mathbf{v}_f \\ \hline \mathbf{p} \\ \hline \mathbf{u}_s \\ \hline \mathbf{u}_m \\ \hline \mathbf{F}_{FSI} \\ \hline \mathbf{F}_m
\end{array}\right) = \mathbf{b}. \tag{6.10}$$

In above, the first two equations correspond to the balance of momentum and continuity in fluid, respectively, the third equation describes the balance of momentum in solid domain, fourth equation is an mesh-updating algorithm, and finally two equations are the coupling equations for fluid-structure, and solid-mesh algorithm, respectively. Symbols $\times$ and $\circ$ indicate non-constant and constant entries of the matrix, respectively, and $\otimes$ indicates terms arising due to linearization of the nonlinear equation due to mesh dynamics.

7 Fluid-structure interaction benchmark problem

We visit the benchmark problem described in [10]. The benchmark problem involves the solution of flow past a rigid cylinder with a nonlinear elastic beam attached at the downstream side of the cylinder (7.2.1).

Three different sets of results are made available in this benchmark problem

1. Computation Fluid Dynamics (CFD): solution to the flow problem under various Reynold numbers without any interaction from a structure. The quantities used for comparison are the lift and drag forces acting on the submerged structure (cylinder and the elastic beam).
2. Computation Solid Mechanics (CSM): solution to the behavior of the nonlinear elastic beam under self-weight without the presence of the fluid. The quantities used for comparison are the deflection of the center midpoint of the tip of the beam.
3. Fluid-structure interaction (FSI): the coupled fluid-structure interaction problem. The quantities used for comparison are the lift and drag forces acting on the beam and cylinder, and the deflections at the end of the beam at its neutral axis in the undeformed configuration.

When a periodic solution is obtained, the mean-value, amplitude, and the frequency of the quantity of interest are compared. These are defined as

$$\text{mean} = \frac{1}{2}\left(\max + \min\right), \tag{7.1}$$

$$\text{amplitude} = \frac{1}{2}\left(\max - \min\right), \tag{7.2}$$

$$\text{frequency} = \frac{1}{T}, \tag{7.3}$$

where "min" and "max" are the minimum and maximum values of quantities of interest, and T is the period.

The computer code is written in the `C++` programming language compiled with `gcc 4.4.1`. Portable, Extensible, Toolkit for Scientific computation (PETSc) [1] is used as the primary package for performing numerical operations.

7.1 Fluid Verfication (CFD)

In this section, we present the results obtained for the partial computational tests corresponding to the fluid solver. The fluid of in these examples is a incompressible Newtonian fluid with a uniform density of $\rho_f = 1000$, and kinematic viscosity of $\mu_f = 1.0$. The domain setup is shown in Figure 7.1.1.

The inflow condition is prescribed as

$$\mathbf{v}_f = \begin{cases} v_f(0, x_2)\left[1 - \cos\left(\frac{\pi}{2}t\right)\right] & t < 2.0 \\ v_f(0, x_2) & t \geq 2.0 \end{cases}, \tag{7.4}$$

where $v_f(0, x_2)$ velocity profile is given as

$$v_f(0, x_2) = \frac{6}{0.1681} X_2(0.41 - X_2)\bar{U}, \tag{7.5}$$

and $\bar{U}$ is a given mean inflow velocity. Three different values of $\bar{U} = 0.2, 1.0$, and 2.0 are considered which, based on the diameter of the cylinder, correspond to Reynolds numbers of $20, 100$, and 200, respectively.

A traction-free outflow (also referred to as 'stress-free' or 'do nothing') condition is enforced weakly on the far right side of the domain.

The finite element mesh used for the solution of the incompressible Navier-Stokes equations in the subsequent sections is shown in Figure 7.1.2. There are a total of 3610 bilinear elements, resulting in a total of $11,451$ degrees of freedom.

7.1.1 Partial Test 1 (CFD1)

The second-order Crank-Nicolson scheme ($\theta = 0.5$) is used for time integration with a time-step of $\Delta t = 0.01$. The flow problem with mean flow value of $\bar{U} = 0.2$ ($Re = 20$) ultimately results in a steady state solution. The time history of the drag and lift forces acting on the cylinder and the beam are shown in Figure 7.1.3. The corresponding stead-state values for drag and lift forces (Table 7.1.1) are in good agreement with those reported in [10].

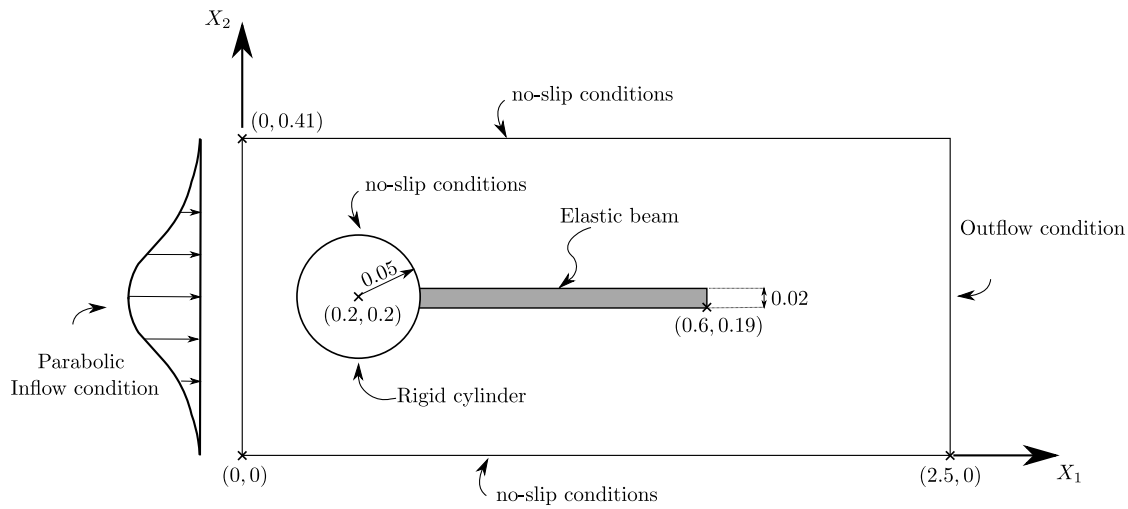

Figure 7.1.1: Schematics of the benchmark FSI problem.

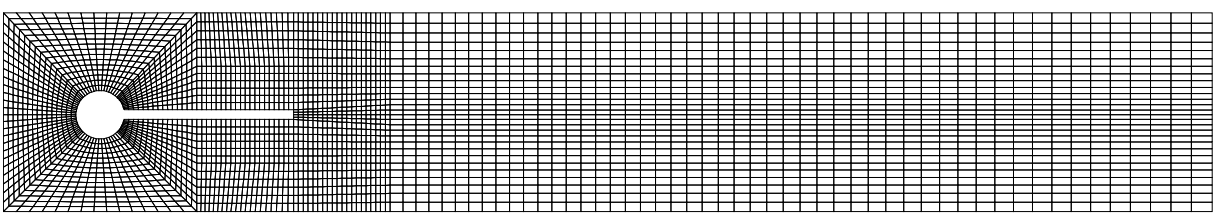

Figure 7.1.2: Finite element mesh used for the solution of the N-S equations.

7.1.2 Partial test 2 (CFD2)

In this test, mean flow value of $\bar{U} = 1.0$ is tested which corresponds to a Reynolds number of 100.

The results in this section are obtained using the second-order Crank-Nicolson scheme with a time-step of $\Delta t = 0.01$. Figure 7.1.4 shows time-history of the drag and lift forces acting on the cylinder and the beam. As in the case of CFD1, ultimately a steady-state solution is obtained. The obtained steady-state values for drag and lift forces acting on the submerged structure is tabulated in Table 7.1.2 and compared with those published in [10].

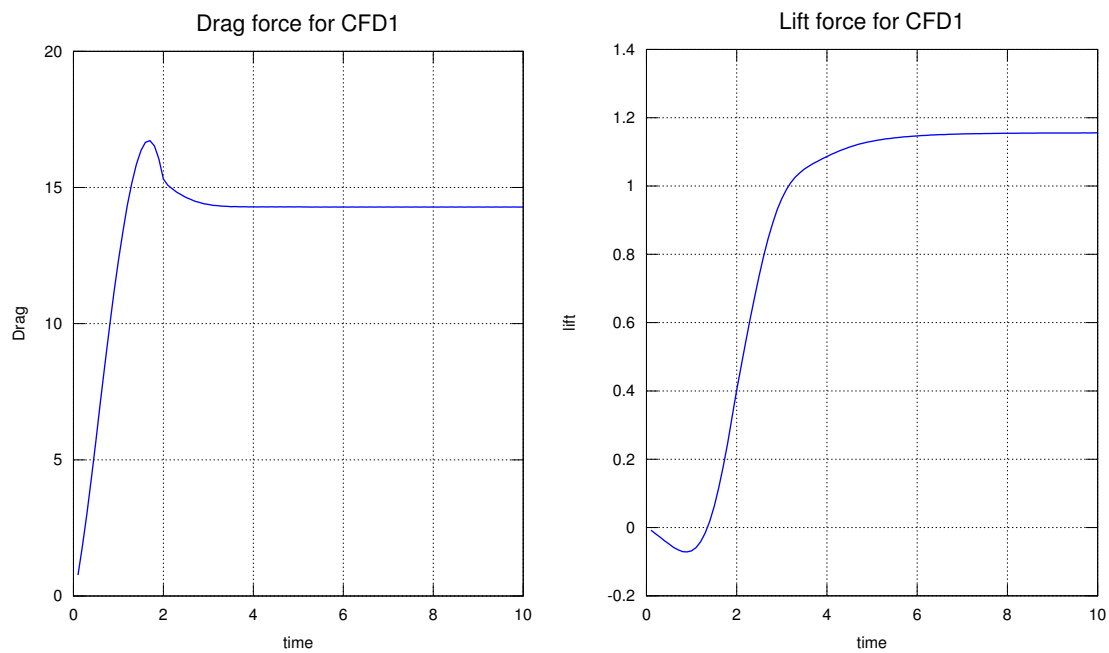

Figure 7.1.3: Time history of drag and lift forces for CFD1. Time integraed using Crank-Nicolson, $\Delta t = 0.01$

Table 7.1.1: Results for CFD1

CFD1	Drag	Lift
Present	14.285	1.156
Reference	14.29	1.119

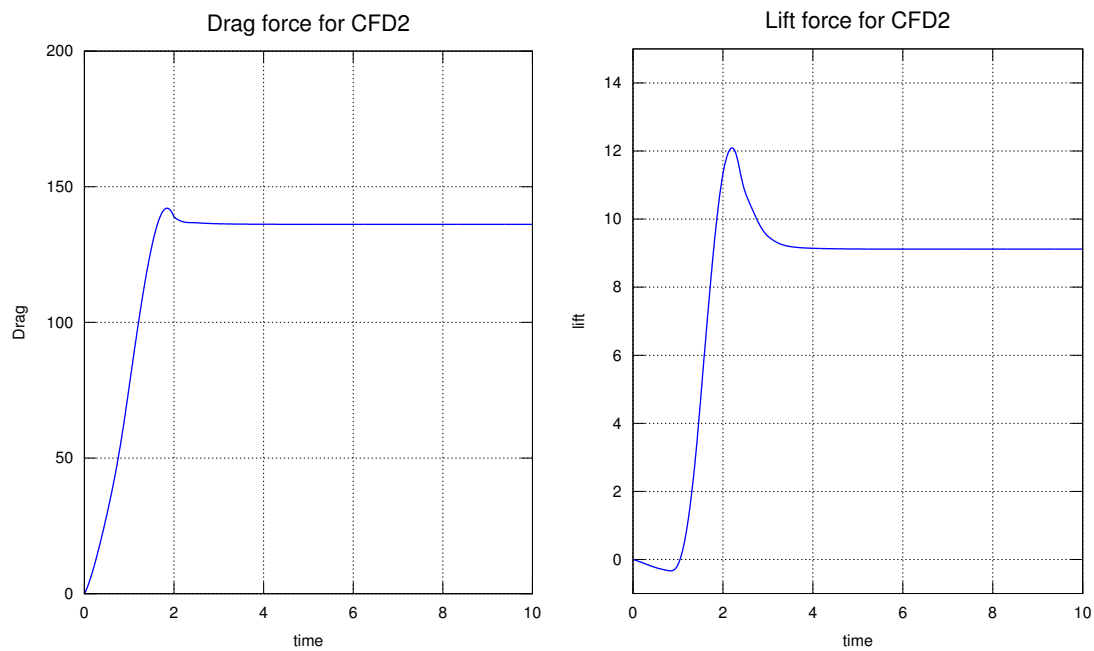

Figure 7.1.4: History of drag and lift forces for CFD2

7.1.3 Partial test 3 (CFD3)

The third and final CFD test, a flow with a mean value of $\bar{U} = 2$ is prescribed which corresponds to a flow with a Reynolds number of 200. The results described in this section are ran with the second-order Crank-Nicolson scheme with a time-stepping size of $\Delta t = 0.01$.

The time history of the drag and lift forces acting on the submerged structure is shown in Figures 7.1.5. These results are tabulated in Table 7.1.3 and compared with those published in [10].

Table 7.1.2: Results for CFD2

CFD1	Drag	Lift
Present	136.13	9.119
Reference	136.7	10.53

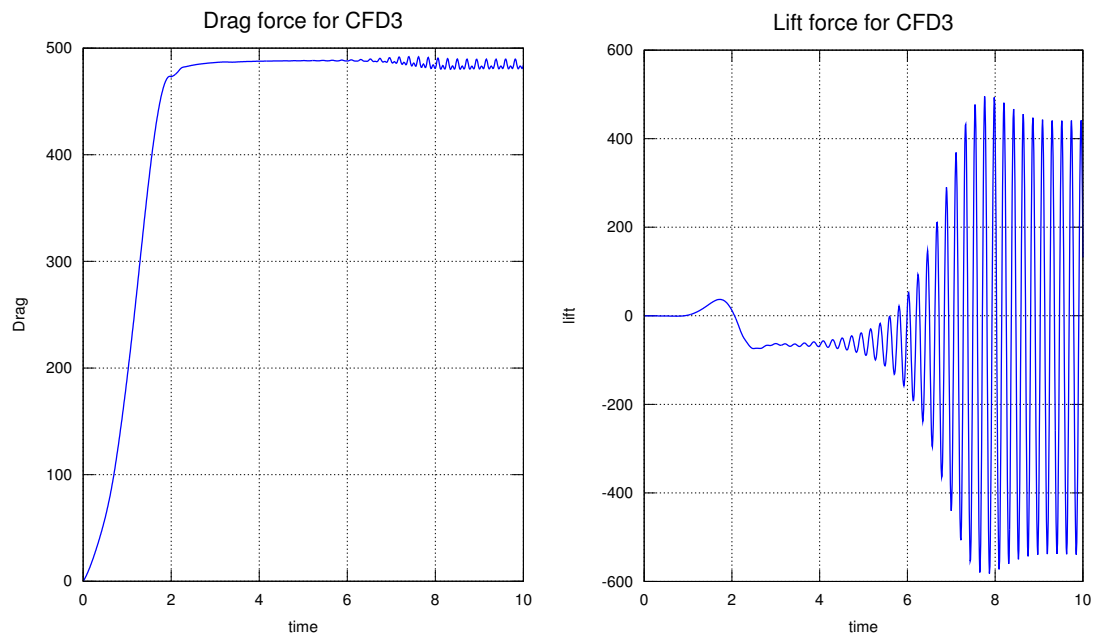

Figure 7.1.5: History of drag and lift forces for CFD3

Table 7.1.3: CFD3 results

Case	Drag	Lift
Present	$484.37 \pm 3.865[4.329]$	$-81.44 \pm 493.36[4.55]$
Reference	$439.45 \pm 5.6173[4.3956]$	$-11.893 \pm 437.81[4.3956]$

7.2 Solid verification (CSM)

In this section, we consider the structural component of the benchmark problem discussed in Section 7. The dimensions of the problem are shown in Figure 7.2.1. In

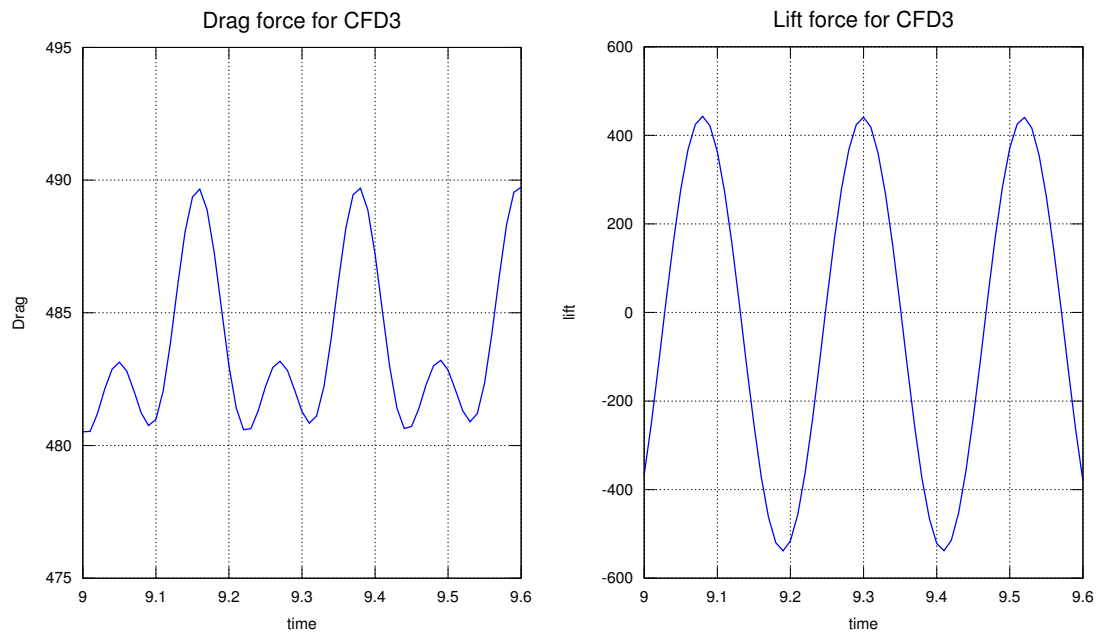

Figure 7.1.6: History of drag and lift forces for CFD3 – magnified

these problems, the driving force is only the self-weight of the beam. In all following problems, the gravitational constant and Lamé constant ν^s are taken to be $g = -2$ and $\nu^s = 0.4$. In all simulations, bilinear quadratic elements are used, and the beam

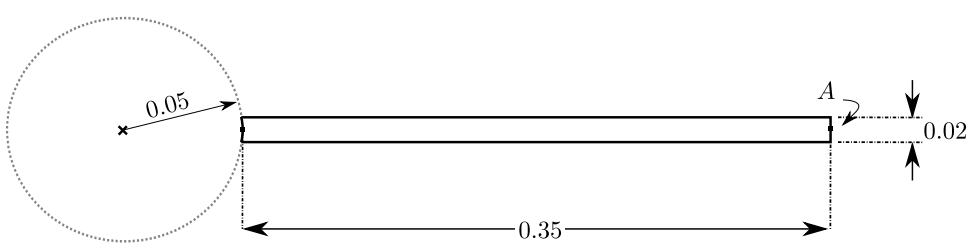

Figure 7.2.1: Schematics of the benchmark CSM problem.

is assumed to be perfectly rectangular in its un-deformed configuration (neglecting the circular inclusion) for convenience.

The quantity used for verification is the displacement of point A in beam (see Figure 7.2.1).

7.2.1 Partial test 1 (CSM1)

This test involves the analysis of the elastic beam under self-weight without including the intertial effects. Elastic modulus is taken to be $E^s = 1.4 \times 10^6$. We consider 4 discretization levels to verify that the solution converges with mesh refinement. The coarsest mesh size (35×4) is the one used in the coupled fluid-structure interaction test problem described in the next section. The displacements at point A of beam for various discretization levels are tabulated in Table 7.2.1 and compared with the reference values available in [10].

Table 7.2.1: Results for CSM1

Resolution	No. of elements	ndof	u_x of A [$\times 10^{-3}$]	u_y of A [$\times 10^{-3}$]
35×4	140	360	-5.600	-58.373
100×12	1,200	2,626	-6.848	-64.438
200×24	48,000	10,050	-7.019	-65.248
300×50	15,000	30,702	-7.059	-65.433
Reference	–	–	-7.187	-66.10

7.2.2 Partial test 2 (CSM2)

In this test, we again consider elastic beam under self-weight without including the intertial effects. Elastic modulus is taken to be $E^s = 5.6 \times 10^6$. The displacements at point A of beam for various discretization levels are tabulated in Table 7.2.2 and compared with the reference values available in [10].

7.2.3 Partial test 3 (CSM3)

In the last partial test for the solid, the elastic modulus of the beam is taken as $E^s = 1.4 \times 10^6$ and the inertial effects are included. The obtained results are tabulated in Table 7.2.3 for two disretization levels. The first discretization corresponds to the discretization used for solving the fluid-structure interaction problem considered in the next section.

Table 7.2.2: Results for CSM2

Resolution	No. of elements	ndof	u_x of A [$\times 10^{-3}$]	u_y of A [$\times 10^{-3}$]
35×4	140	360	-0.362	-14.901
100×12	1,200	2,626	-0.446	-16.527
200×24	4,800	10,050	-0.458	-16.745
300×50	15,000	30,702	-0.460	-16.795
Reference	–	–	-0.4690	-16.97

The time-history of the vertical and lateral deflections of point A on the beam for the coarsest mesh are shown in Figures 7.2.2 and 7.2.3, respectively.

Table 7.2.3: Results for CSM3

Resolution	No. of elements	ndof	u_x of A [$\times 10^{-3}$]	u_y of A [$\times 10^{-3}$]
35×4	140	360	$-11.204 \pm 11.2035[1.15]$	$-56.652 \pm 57.798[1.15]$
300×18	5,400	11,438	$-14.226 \pm 14.228[1.09]$	$-63.558 \pm 64.372[1.11]$
Reference	–	–	$-14.305 \pm 14.305[1.0995]$	$-63.607 \pm 65.160[1.0995]$

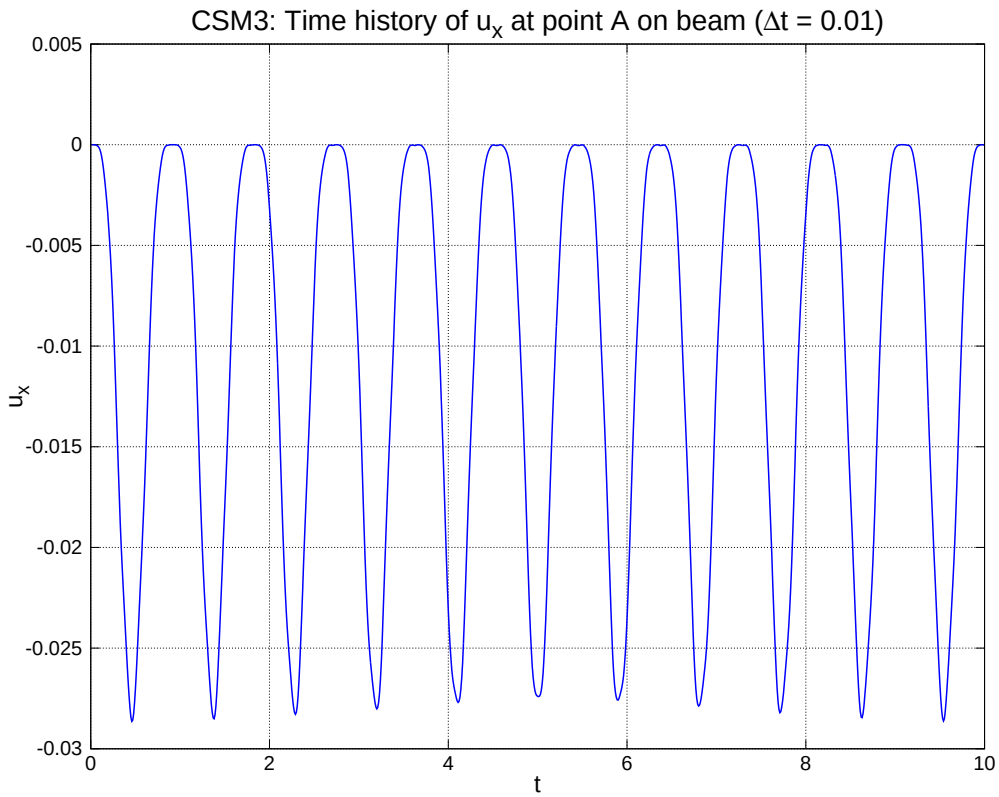

Figure 7.2.2: Time history of u_x of point A on beam

.

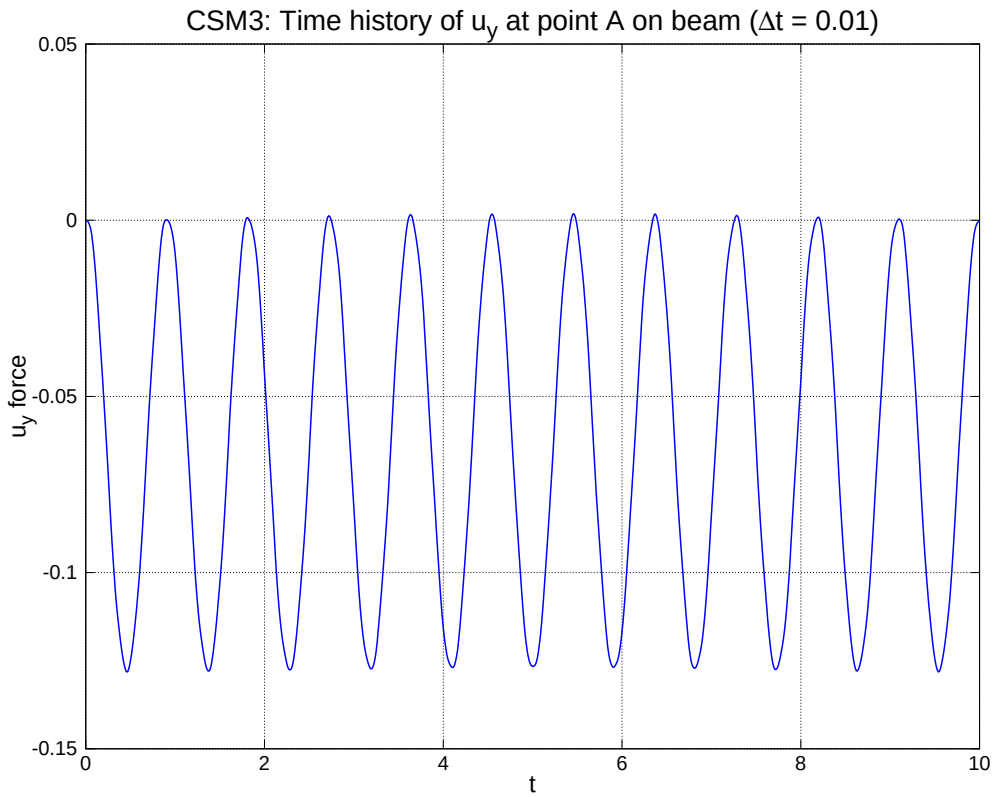

Figure 7.2.3: Time history of u_y of point A on beam

.

8 Monolithic formulation verification

In this section we consider the fully coupled problem of flow passed a nonlinear elastic beam attached to a cylinder. The parameter settings for the fluid-structure interaction test cases are listed in Table 8.0.4.

Table 8.0.4: FSI parameter settings

Parameters	FSI1	FSI2	FSI3
$\rho_s[10^3]$	1	10	1
$E_s[10^6]$	1.4	1.4	5.6
$\rho_f[10^3]$	1	1	1
ν_f	1	1	1
$\bar{U}$	0.2	1	2

8.1 Fluid-structure interaction CASE 1 (FSI1)

The time history of the drag and lift forces acting on the submerged structure are shown in Figures 8.1.1 and 8.1.2, respectively. These results are obtained using the second-order accurate Crank-Nicolson (CN) scheme with a time-step of $\Delta t = 0.01$. The solution reaches what looks to be a steady state solution before exhibiting signs of instability as can be seen in Figures 8.1.1.

The same problem is revisited using the Backward-Euler (BE) time-integration scheme with a time-step size of $\Delta t = 0.001$. The graphs of lift and drag forces are shown in Figures 8.1.5 and 8.1.6, respectively, and deflection in the horizontal and vertical direction of point A is shown in Figures 8.1.7 and 8.1.8, respectively.

The steady-state values of the solution are tabulated in Table 8.1.1 and compared to those listed in [10]. The discrepancy of the two solutions can be explained by the rather coarse mesh (35×4) used for spacial discretization of the beam.

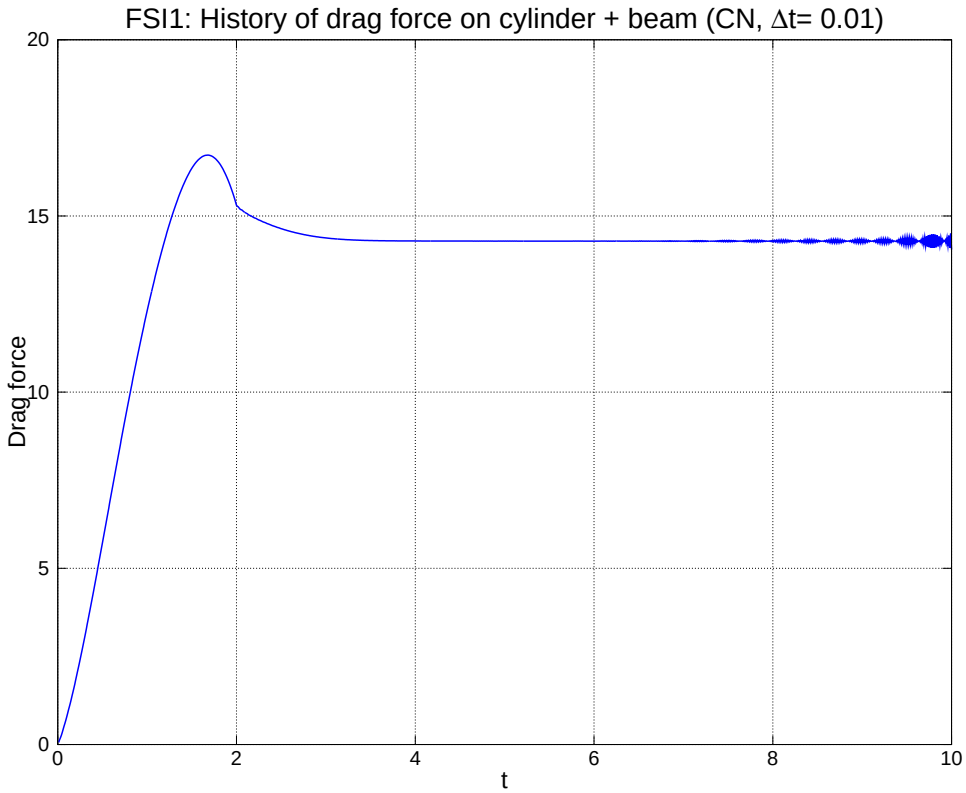

Figure 8.1.1: History of drag force for FSI1 using Crank-Nicolson time integration scheme with $\Delta t = 0.01$ showing instability towards the end of the graph

.

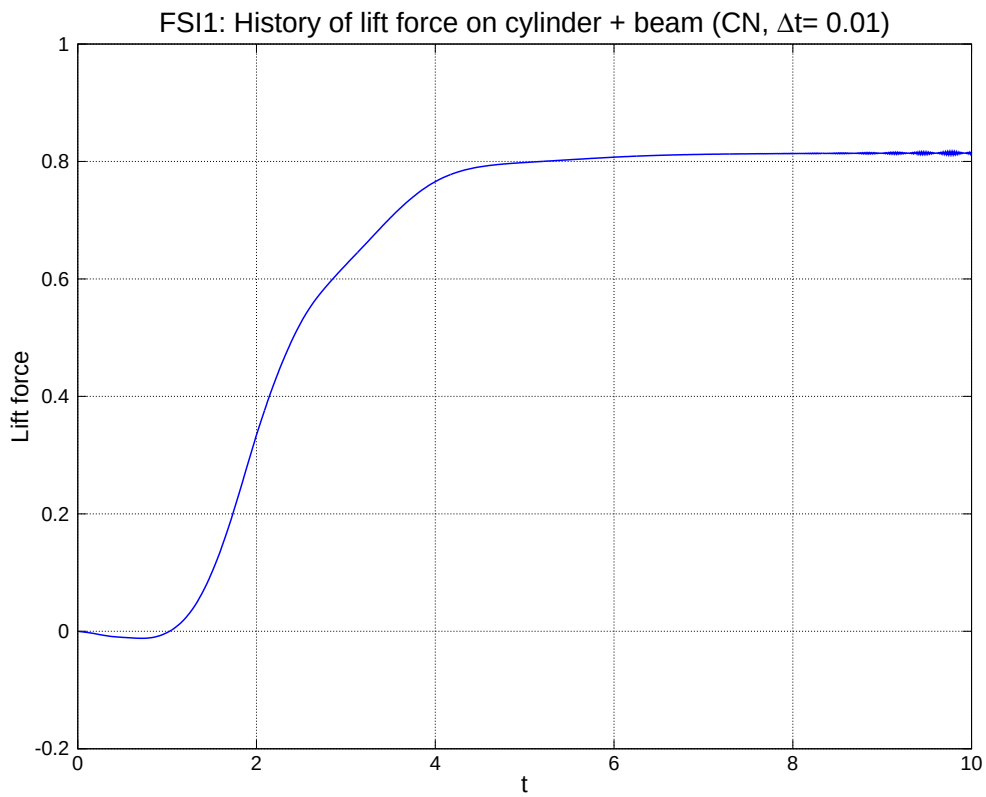

Figure 8.1.2: History of lift force for FSI1 using Crank-Nicolson time integration scheme with $\Delta t = 0.01$

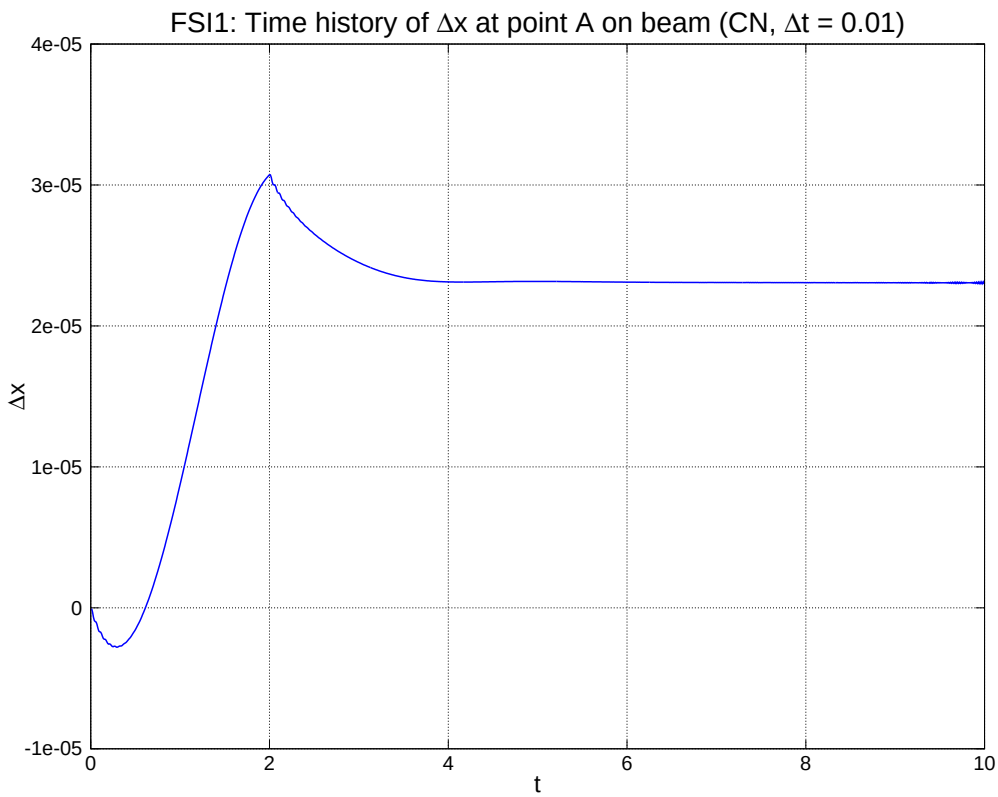

Figure 8.1.3: History of Δu_1 at tip of beam using Crank Nicolson time integration scheme with $\Delta t = 0.01$ – FSI1

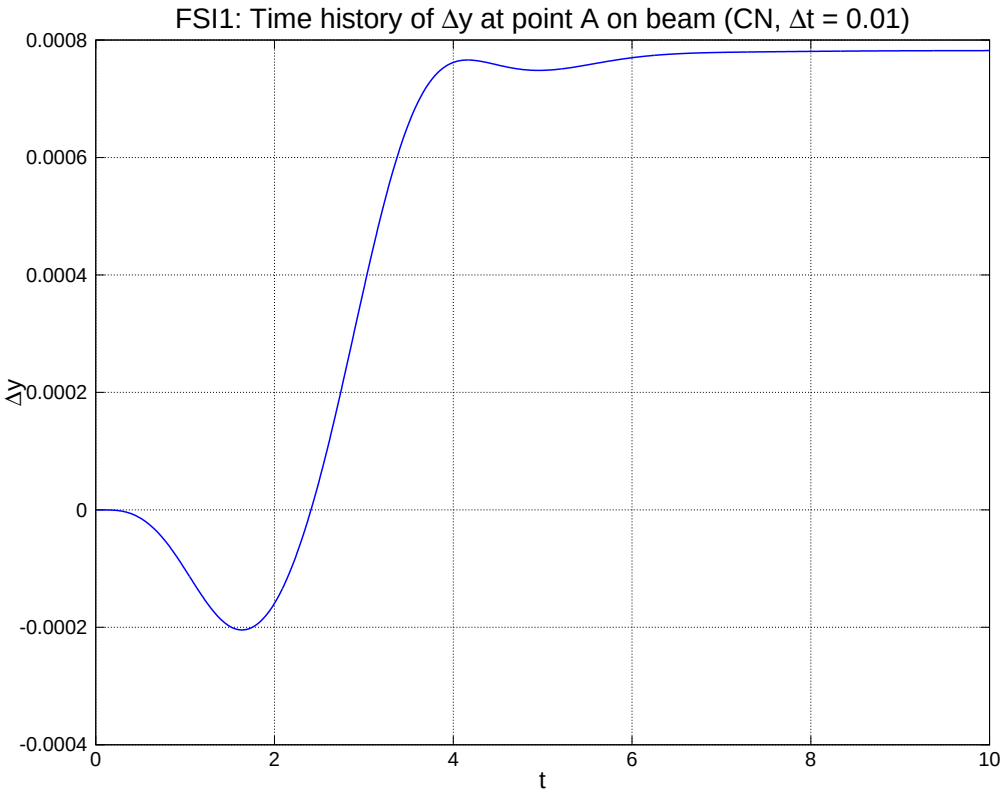

Figure 8.1.4: History of Δu_2 at tip of beam using Crank-Nicolson time integration scheme with $\Delta t = 0.01$ – FSI1

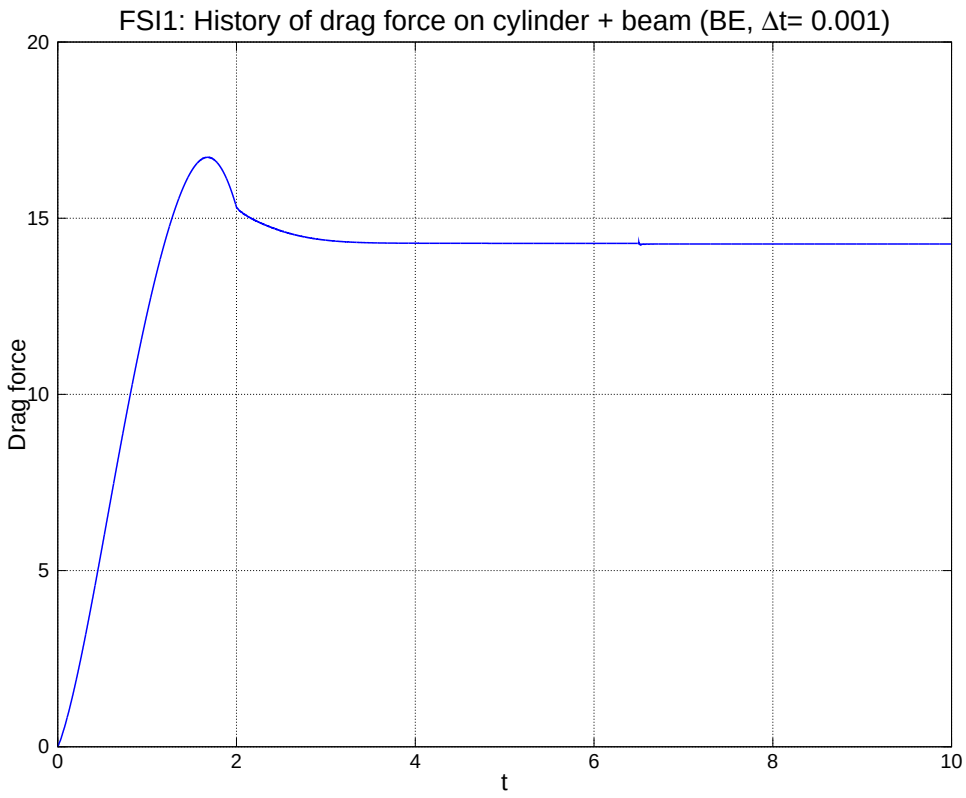

Figure 8.1.5: History of drag force for FSI1 using Backward-Euler scheme with $\Delta t = 0.001$

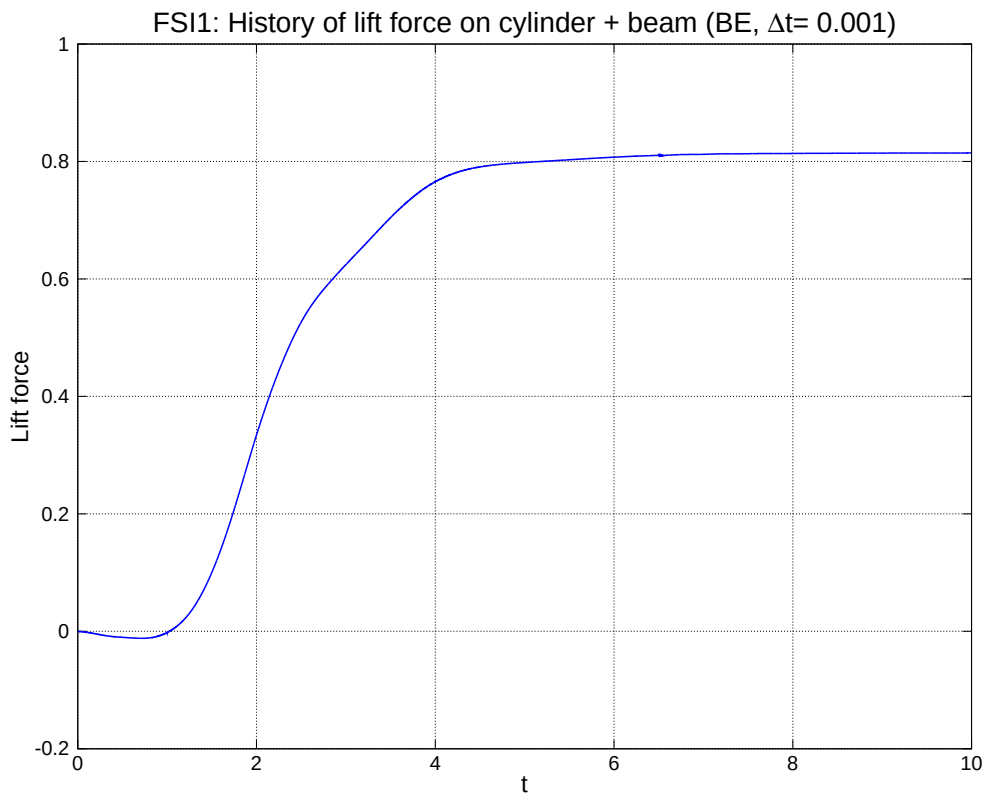

Figure 8.1.6: History of lift force for FSI1 using Backward-Euler scheme with $\Delta t = 0.001$

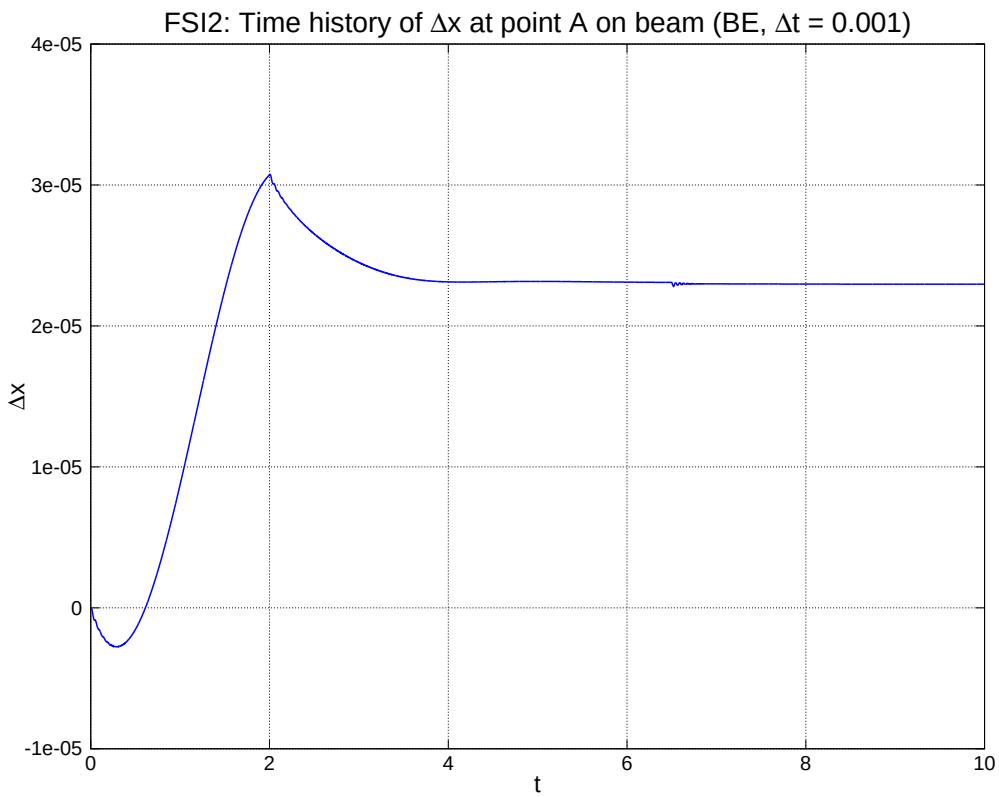

Figure 8.1.7: History of Δu_1 at tip of beam using Backward-Euler time integration scheme with $\Delta t = 0.001$ – FSI1

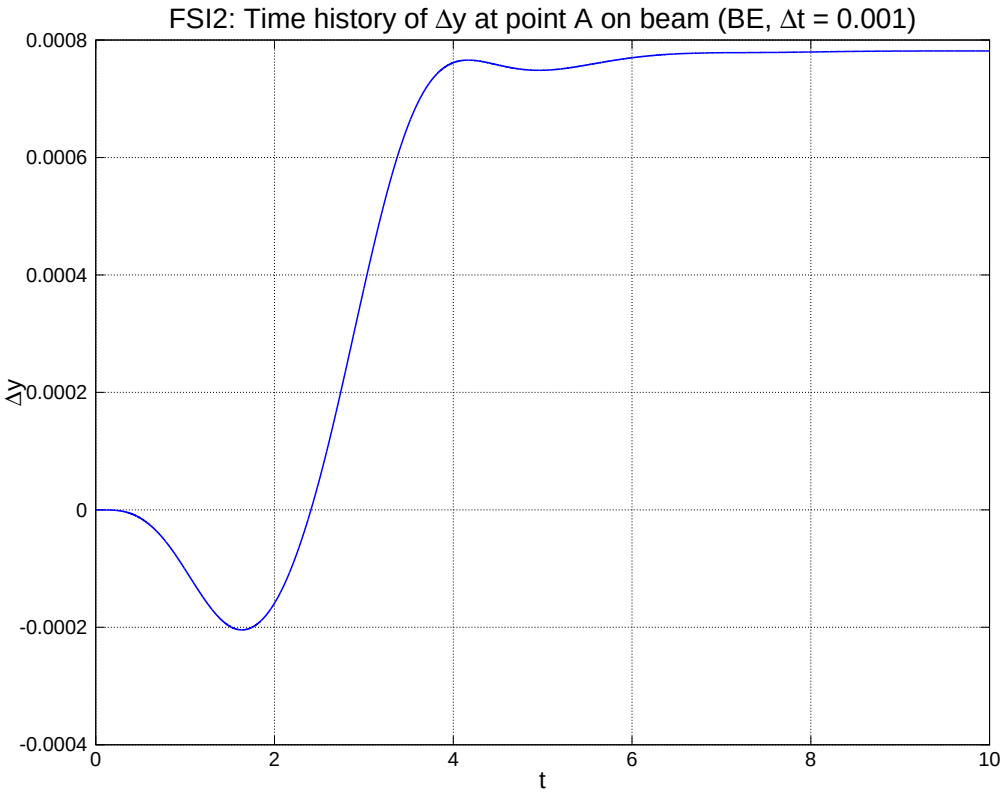

Figure 8.1.8: History of Δu_2 at tip of beam using Backward-Euler time integration scheme with $\Delta t = 0.001$ – FSI1

Table 8.1.1: FSI1 results using Backward-Euler

Case	u_x of A $[10^{-3}]$	u_y of A $[10^{-3}]$	Drag	Lift
Present (BE)	0.0230	0.7815	14.267	0.8145
Reference	0.0227	0.8209	14.295	0.7638

8.2 Fluid-structure interaction CASE 1 (FSI2)

These results in this section are obtained using the second-order accurate Crank-Nicolson (CN) scheme with a time-step of $\Delta t = 0.01$.

The time history of the drag and lift forces acting on the submerged structure are shown in Figures 8.2.1 and 8.2.2, respectively. The time history of the deflections at point A of the beam are plotted in Figures 8.2.3 and 8.2.4. As it can be shown in these figures, the beam experiences significant deformations. An isolated snapshot of the computational mesh at a point in which the beam experiences its maximum magnitude of deformation is shown in Figure 8.2.6.

The obtained results are in good agreement to those published in [10] (Table 8.2.1).

Table 8.2.1: FSI2 results

Case	u_x of A $[10^{-3}]$	u_y of A $[10^{-3}]$	Drag	Lift
Present (BE)	$-13.42 \pm 12.08[3.85]$	$1.40 \pm 76.49[3.85]$	$213.20 \pm 71.80[2.0]$	$-0.15 \pm 218.26[2.0]$
Reference	$-14.58 \pm 12.44[3.8]$	$1.23 \pm 80.6[2.0]$	$208.83 \pm 73.75[3.8]$	$0.88 \pm 234.2[2.0]$

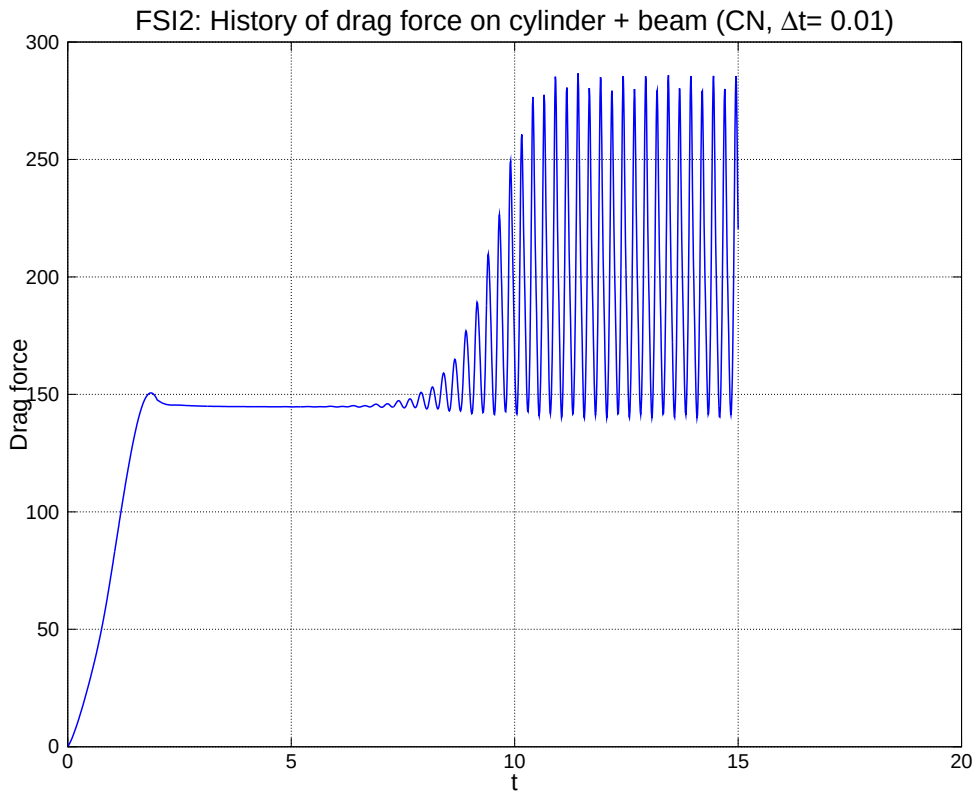

Figure 8.2.1: (FSI2) History of drag force using Crank-Nicolson time integration scheme with $\Delta t = 0.01$

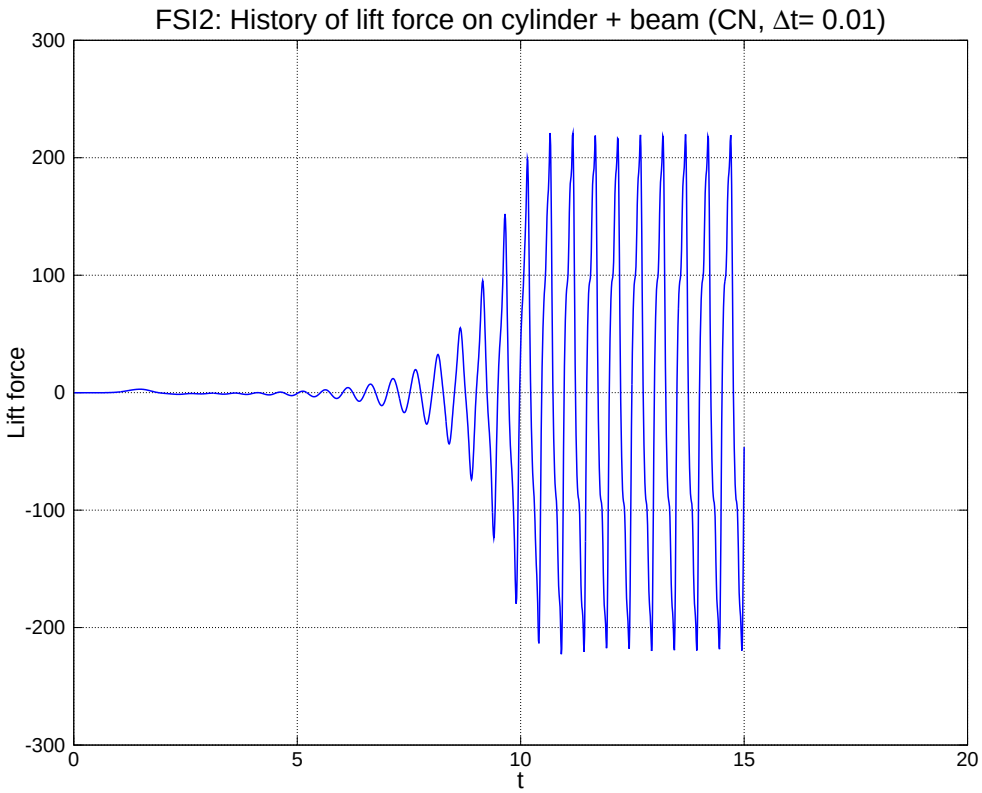

Figure 8.2.2: (FSI2) History of lift force using CN scheme with $\Delta t = 0.01$

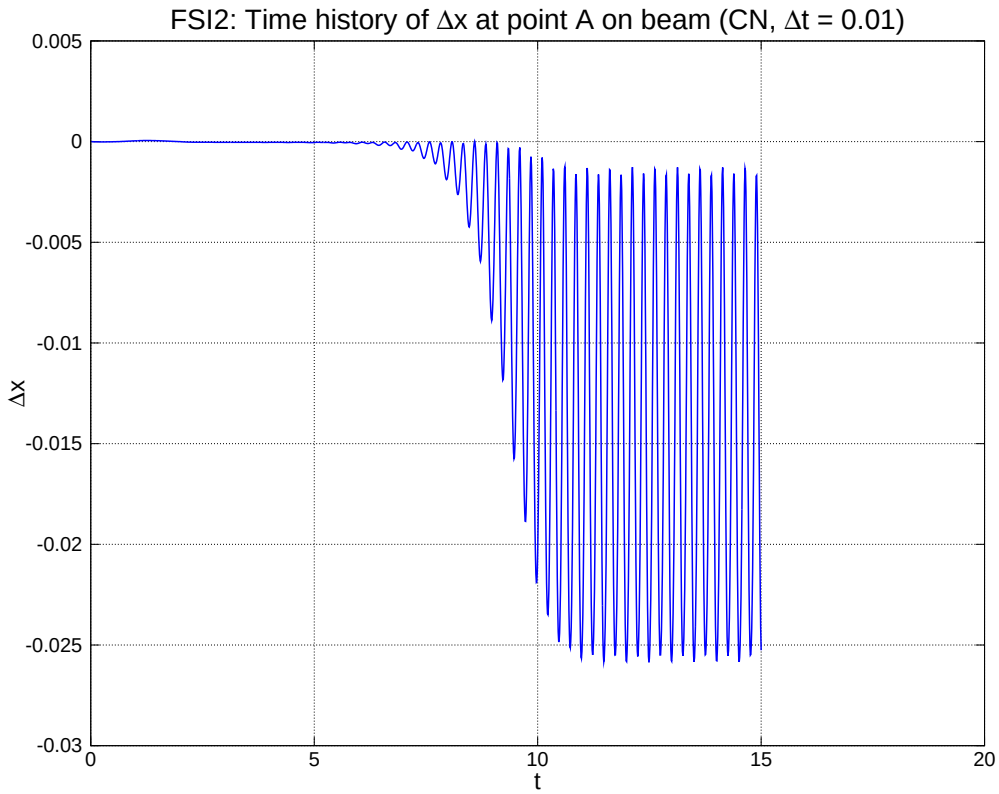

Figure 8.2.3: (FSI2) History of Δu_1 at point A on beam using Crank-Nicolson time integration scheme with $\Delta t = 0.01$

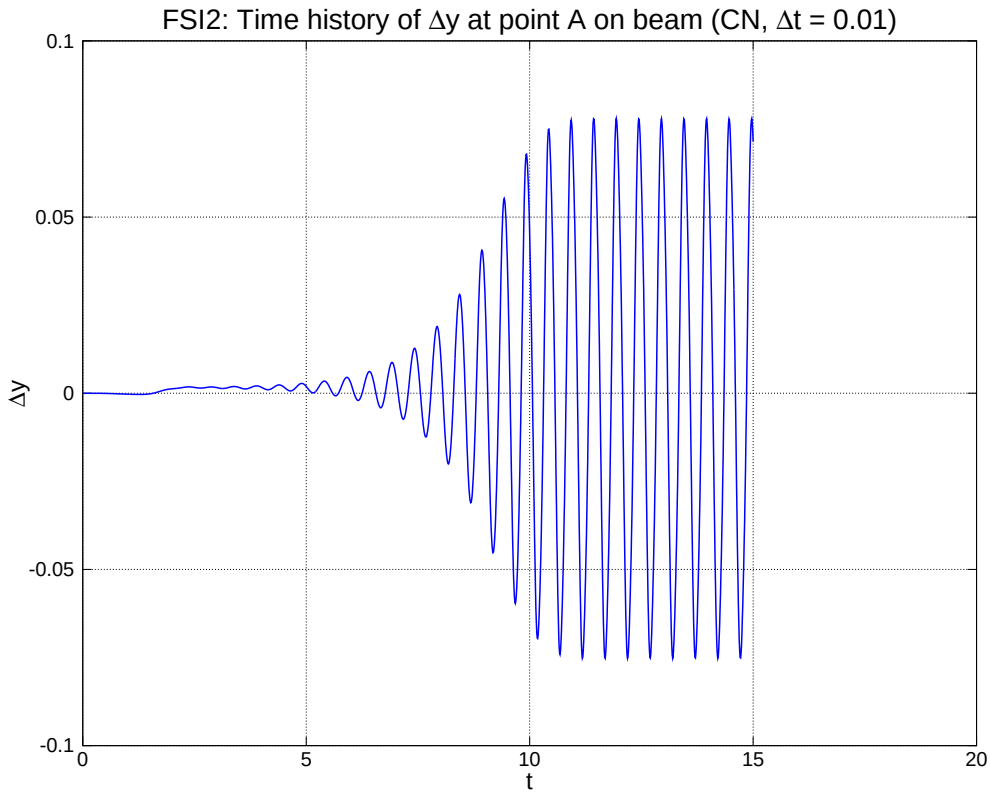

Figure 8.2.4: (FSI2) History of Δu_2 at point A on beam using Crank-Nicolson time integration scheme with $\Delta t = 0.01$

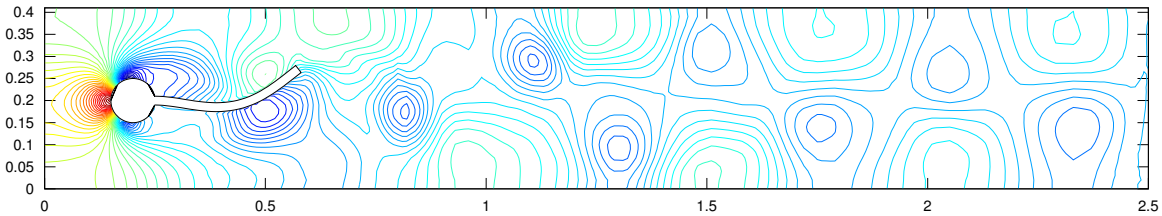

Figure 8.2.5: Snapshot of pressure field at $t = 15$ (CN, $\Delta t = 0.01$)

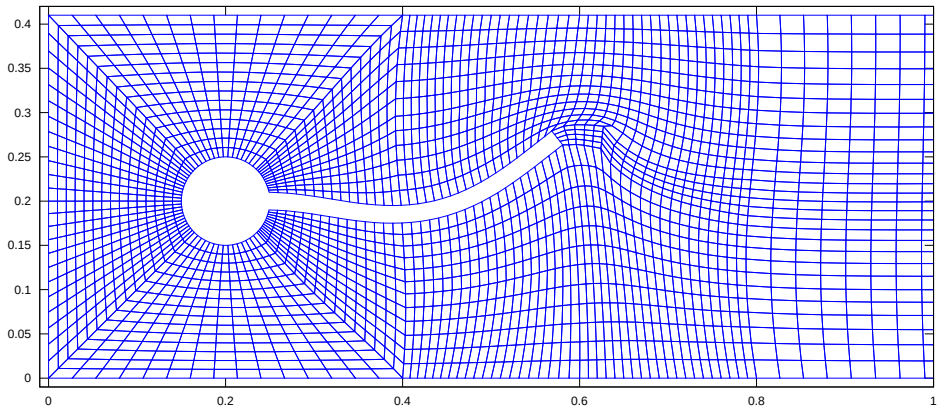

Figure 8.2.6: Snapshot of computational mesh at $t = 15$ (CN, $\Delta t = 0.01$)

9 Work to be done

In this report, we have implemented the ALE formulation for analyzing fluid-structure interaction problems. The obtained results so far have been in good agreement to other available published results. Below, we summarize some of the ongoing work in progress:

1. Numerical instabilities were experienced when a second-order accurate time-stepping scheme was employed for analyzing the fully coupled fluid-structure interaction problem. The cause for the numerical instability is being studied right now.

2. The sea-bed scour problem involves a free-surface. We are considering developing and implementing in the code an appropriate method for tracking free surface.

3. The coupled problem is very computationally expensive. In order to obtain results in a timely manner, a parallel implementation of the code will be considered.

References

[1] Satish Balay, Jed Brown, Kris Buschelman, William D. Gropp, Dinesh Kaushik, Matthew G. Knepley, Lois Curfman McInnes, Barry F. Smith, and Hong Zhang. PETSc Web page, 2011. http://www.mcs.anl.gov/petsc.

[2] S. Étienne, A. Garon, and D. Pelletier. Perspective on the geometric conservation law and finite element methods for ale simulations of incompressible flow. *Journal of Computational Physics*, 228(7):2313 – 2333, 2009.

[3] Ch. Förster, W. A. Wall, and E. Ramm. On the geometric conservation law in transient flow calculations on deforming domains. *International Journal for Numerical Methods in Fluids*, 50(12):1369–1379, 2006.

[4] Christiane Frster, Wolfgang A. Wall, and Ekkehard Ramm. Artificial added mass instabilities in sequential staggered coupling of nonlinear structures and incompressible viscous flows. *Computer Methods in Applied Mechanics and Engineering*, 196(7):1278 – 1293, 2007.

[5] P.M. Gresho, R.L. Sani, and M.S. Engelman. *Incompressible Flow and the Finite Element Method: Advection-Diffusion and Isothermal Laminal Flow.* John Wiley and Sons, 1998.

[6] E. Onate, J. Garcia, S.R. Idelsohn, and F. Del Pin. Finite calculus formulations for finite element analysis of incompressible flows. Eulerian, ALE and Lagrangian approaches. *Comput. Methods Appl. Mech. Engrg.*, 195:3001–3037, 2006.

[7] Michael Schäfer, Marcus Heck, and Saim Yigit. An implicit partitioned method for the numeric al simulation of fluid-structure interaction. In Hans-Joachim Bungartz and Michael Schfer, editors, *Fluid-Structure Interaction*, volume 53 of *Lecture Notes in Computational Science and Engineering*, pages 171–194. Springer Berlin Heidelberg, 2006.

[8] T.E. Tezduyar. Stabilized finite element formulations for incompressible flow computations. *Advances in Applied Mechanics*, 28:1 – 44, 1991.

[9] P. D. Thomas and C. K. Lombard. Geometric conservation law and its application to flow computations on moving grids. *AIAA Journal*, 17(10):1030–1037, 1979.

[10] Stefan Turek and Jaroslav Hron. Proposal for numerical benchmarking of fluid-structure interaction between an elastic object and laminar incompressible flow. In Hans-Joachim Bungartz and Michael Schfer, editors, *Fluid-Structure Interaction: Modeling, Simulation, Optimisation*, volume 53 of *Lecture Notes in Computational Science and Engineering*, pages 371–385. Springer Berlin Heidelberg, 2006.